# Advanced Biopolymer–Based Soil Strengthening Binder with Trivalent Chromium–Xanthan Gum Crosslinking for Wet Strength and Durability Enhancement

Minhyeong Lee, Ph.D.[1]; Ilhan Chang, Ph.D., A.M.ASCE[2]; and Gye-Chun Cho, Ph.D.[3]

**Abstract:** Xanthan gum (XG) is an effective soil-binding material for enhancing the geotechnical engineering performance of soil. Due to the hydrophilicity of XG, however, its ineffectiveness as a soil-strengthening agent in wet conditions and the associated durability concerns continue to be obstacles to the implementation of XG soil treatment. Here, we investigated the effect of trivalent chromium ($Cr^{3+}$) crosslinking on the rheology of XG hydrogels, and consequent variations in the unconfined compressive strength of XG–$Cr^{3+}$-treated soil. Rheological tests revealed that the crosslinking of $Cr^{3+}$ initially increased the yield stress of the XG gel; as the gel cured, the XG–$Cr^{3+}$ gel lost its viscoelasticity and became stiffer and more elastic. With increased $Cr^{3+}$ and XG concentrations, the time-controllable gelation enhanced the unconfined compressive strength of the sandy soil in a hydrated state. Furthermore, the crosslinking of XG and $Cr^{3+}$ reduced the swelling of the XG gel and increased strength durability of XG–$Cr^{3+}$-treated soil under prolonged saturation conditions. Due to the fact that $Cr^{3+}$ crosslinking effectively improved the wet strength and durability without additional dehydration or heat treatment, this method can expand the applicability of XG soil treatment, such as injection grouting or backfill material for various geotechnical engineering structures. **DOI: 10.1061/JMCEE7.MTENG-16123.** 

**Author keywords:** Xanthan gum (XG); Trivalent chromium; Crosslinking; Soil improvement; Wet strength; Durability; Grouting material.



## Introduction

Significant environmental changes such as global warming, heat waves, and extreme precipitation have frequently been followed in recent years by numerous geotechnical engineering hazards (Chang et al. 2019; Hansen et al. 2010). In the field of geotechnical engineering, conventional soil stabilizers, such as cement, pose environmental concerns including carbon dioxide emissions and pH-altering effects (Worrell et al. 2001; Zheng et al. 2019). In order to promote sustainable development, geotechnical engineers have investigated bio-based soil remediation techniques (Chang et al. 2016b; DeJong et al. 2010; Whiffin et al. 2007).

Biopolymer soil treatment formulates a strategy for environmentally friendly soil improvement by primarily employing exocultivated biopolymers from living organisms such as bacteria, fungi, and plants (Chang et al. 2016b). Among biopolymers, xanthan gum (XG) has demonstrated superior enhancement in engineering properties of soil including compressive/shear strength (Cabalar and Canakci 2011; Chang et al. 2015a, 2021; Kang et al. 2019; Lee et al. 2021b; Qureshi et al. 2017), tensile strength (Jiang et al. 2022), and erosion resistance (Kang et al. 2021; Ko and Kang 2018), along with reduced hydraulic conductivity (Cabalar et al. 2017; Lee et al. 2021a; Sujatha et al. 2020) and increased vegetation (Chang et al. 2015c; Tran et al. 2019). Particularly, XG offers promising prospects for practical applications (Kang et al. 2021; Seo et al. 2021) because it provides substantial strengthening even in small amounts (i.e., 0.5%–1% of the soil mass), and its affordability increases its economic feasibility (Ayeldeen et al. 2016; Chang et al. 2020).

However, even though these completed studies have shown promising results when XG and XG-based compounds are used as a soil stabilizer, XG soil treatments have two main challenges related to moisture state and weak-gel property of XG. Due to its hydrophilic nature, XG is extremely sensitive to the presence of water (Casas et al. 2000); therefore, its soil-strengthening effectiveness highly dependent on the soil's moisture content (Lee et al. 2021b, 2022). For example, dehydrated XG-treated soil has a high strength, whereas hydrated (e.g., initially wet or resubmerged) XG-treated soil has a significantly lower strength (Chen et al. 2019; Lee et al. 2021b). In other words, the durability of XG-treated soil dramatically degrades in the presence of water due to strength loss with dissolution and swelling of XG under saturated conditions (Chen et al. 2019; Lee et al. 2022; Soldo et al. 2020). Consequently, despite the benefits of high dry strength and cost-effectiveness, the development of XG soil treatment is hindered by (1) initially low wet strength, and (2) water-vulnerable strength characteristic of XG-treated soil.

XG, which has nongelling (weak-gel) properties in a hydrated state, possesses a number of hydroxyl (-OH) and carboxyl (-COOH) groups, which are amenable for chemical modification with successive improvement in its physicochemical properties (Patel et al. 2020). Thus, numerous studies have been studied

[1]Postdoctoral Researcher, Disposal Performance Demonstration Research Division, Korea Atomic Energy Research Institute, Daejeon 34057, Republic of Korea. ORCID: https://orcid.org/0000-0002-2148-0766. Email: leemh@kaeri.re.kr

[2]Associate Professor, Dept. of Civil Systems Engineering, Ajou Univ., Suwon 16499, Republic of Korea. ORCID: https://orcid.org/0000-0001-8369-0606. Email: ilhanchang@ajou.ac.kr

[3]Professor, Dept. of Civil and Environmental Engineering, Korea Advanced Institute of Science and Technology, Daejeon 34141, Republic of Korea (corresponding author). ORCID: https://orcid.org/0000-0001-8582-9237. Email: gyechun@kaist.edu

Note. This manuscript was submitted on December 6, 2022; approved on March 15, 2023; published online on July 27, 2023. Discussion period open until December 27, 2023; separate discussions must be submitted for individual papers. This paper is part of the ***Journal of Materials in Civil Engineering***, © ASCE, ISSN 0899-1561.

physical/chemical crosslinking methods to induce gelation of XG (Ahmad et al. 2015; Alvarez-Lorenzo et al. 2013; Patel et al. 2020; Riaz et al. 2021) For example, XG showed gel-forming behavior when crosslinked with other biopolymers such as alginate (Fan et al. 2021), chitosan (Argin et al. 2014), locust bean gum (Kennedy et al. 2015), konjac glucomannan (Fan et al. 2008), and starch (Sethi et al. 2020), particularly in the presence of heat. Gelation of XG can occur in the presence of multivalent (i.e., divalent and trivalent) salts (Izawa and Kadokawa 2010; Shibaev et al. 2020).

The majority of divalent ions (e.g., $Ca^{2+}$ and $Ba^{2+}$) can be conjugated with XG under alkaline conditions, whereas trivalent ions (e.g., $Al^{3+}$, $Fe^{3+}$, and $Cr^{3+}$) have a higher crosslink rate across a wider pH range (Ahmad et al. 2015; Sanderson 1981). Especially trivalent chromium ($Cr^{3+}$) has competitiveness over other trivalent cations suitable for XG gelation, owing to its reactivity over a wide pH range, commercial popularity (Marudova-Zsivanovits et al. 2007), and moderate setting (gelation) time for homogeneous gel formation (Lund et al. 1988; Prud'homme et al. 1983). Thus, the XG–$Cr^{3+}$ crosslinking method was actively utilized in enhanced oil recovery to form soft gel as blocking agent using diluted XG solution (0.001%–0.05% by weight) (Avery et al. 1986; Nolte et al. 1992). Moreover, multifarious experimental analyses on kinetics and gelation behavior of the XG–$Cr^{3+}$ crosslinking were carried out using rheometry (Nolte et al. 1992), dynamic light scattering (Rodd et al. 2001), and nuclear magnetic resonance (Hansen and Lund 1995). Nevertheless, the gelation process itself is not well understood, and there are only hypotheses about the gelling mechanism as a formation of dimeric and polymeric ionic bridges (Patel et al. 2020).

Based on the literature, we hypothesized that gelation via $Cr^{3+}$ crosslinking could assist in overcoming the water-related low efficiency of XG-treated soil. The effects of $Cr^{3+}$ crosslinking in highly concentrated XG hydrogel (1%–5% by weight) on gel stiffness and soil-strengthening behavior have not yet been thoroughly investigated. In response, this study utilized $Cr^{3+}$ crosslinking strategy to enhance wet strength and durability of XG-treated soil for the first time to overcome the weakness of previous biopolymer-soil treatment technology. We conducted rheometry to assess rheology and gel formation behavior of XG–$Cr^{3+}$ gel, and unconfined compressive test, and immersion/cyclic wet-dry durability test to evaluate strength performance in XG–$Cr^{3+}$-treated soil.

## Materials and Experimental Programs

### Xanthan Gum Biopolymer

As a base polysaccharide biopolymer, analytical grade XG (CAS: 11138-66-2; Sigma-Aldrich, St. Louis, Missouri) produced by the fermentation of *Xanthomonas campestris* bacterium was utilized. XG is a commercialized nongelling biopolymer that is widely used in the food, cosmetic, and petroleum industries due to its high temperature and pH stability (Butler 2016). García-Ochoa et al. (2000) reported that its molecular structure consists of a repeating linear backbone with anionic-charged trisaccharide side chains.

The negative charge on the side chains of XG derived from carboxyl groups ($COO^-$) facilitates its binding with water molecules, resulting in a strong expansion behavior and high viscosity upon dissolution in water (Hatakeyama and Hatakeyama 1998). Moreover, under static conditions, the XG molecules generate a weak gellike network due to the hydrogen bonding and entanglements induced by the side chains (Moorhouse et al. 1977). Currently, XG is used as a soil-strengthening agent in geotechnical engineering (Chang et al. 2015a; Singh and Das 2020).

### Chromium Nitrate Nonahydrate

As a source of $Cr^{3+}$ ions, extrapure chromium nitrate nonahydrate [$Cr(NO_3)_3 \cdot 9H_2O$, 99%, Daejung Chemical Co., Korea], a crystal with violet hue and high water solubility, was used. $Cr^{3+}$ is the most thermodynamically stable form of chromium, and nearly all naturally occurring chromium in the environment exists in this form (Baruthio 1992). $Cr^{3+}$ is an essential trace element for carbohydrate and lipid metabolism in humans and animals, and it has a less toxic effect than hexavalent chromium ($Cr^{6+}$), one of the most common hazardous heavy-metal ions (Baruthio 1992). Previously $Cr^{3+}$ has been used as an inorganic crosslinker to improve the stability and capabilities of anionic polymers, particularly for oil industry sweep efficiency (Zolfaghari et al. 2006).

### Used Soil: Jumunjin Sand

This study employed Jumunjin sand, the standard sand in South Korea, for its experimental tests. According to the Unified Soil Classification System (USCS), Jumunjin sand is classified as poorly graded sand (SP), with the following soil properties: mean particle size ($D_{50}$) = 0.5 mm, coefficient of uniformity ($C_u$) = 1.63, coefficient of curvature ($C_c$) = 1.08, specific gravity ($G_s$) = 2.65, minimum void ratio ($e_{min}$) = 0.64, and maximum void ratio ($e_{max}$) = 0.95. Fig. 1 depicts the particle size distribution of sand as determined by a laser diffraction particle size analyzer (HELOS/KR-H2487, Sympatec, Clausthal-Zellerfeld, Germany) in accordance with ASTM D4464-15 (ASTM 2020). Before soil specimen preparation, the sand was dehydrated in an oven.

### Preparation of Pure XG and Crosslinked XG–$Cr^{3+}$ Gels

Pure XG hydrogel was produced by dissolving XG powder in deionized water with 1.25%, 2.5%, and 5% $m_x/m_w$ (where $m_x/m_w$ is the ratio of XG mass to water mass) using a laboratory hand-mixer, and crosslinked XG–$Cr^{3+}$ gel was produced by combining pure XG gel and the aqueous $Cr^{3+}$ solution, both prepared as double of the final desired concentration (Table 1).

In detail, pure XG hydrogel of 2.5%, 5.0%, and 10% $m_x/m_w$, and the same amount of aqueous $Cr^{3+}$ solutions with Cr/XG ratios of 0, 15, 30, 60, and 100% (where Cr/XG = ratio of $Cr(NO_3)_3 \cdot 9H_2O$ mass to XG mass) were thoroughly mixed with a laboratory hand-mixer at 20,000 revolutions per minute (rpm) for 30 s. In addition, a small amount of sodium chloride (NaCl, representing 10%

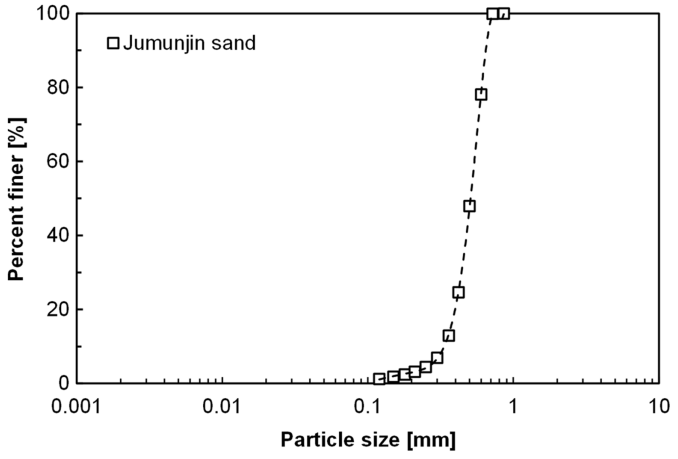


**Fig. 1.** Particle size distribution curves of the used soil.

**Table 1.** Composition for preparation of pure XG and XG–$Cr^{3+}$ gel

| | | | Detailed composition [percentage to water amount (where water is 100%)] | | | | |
|---|---|---|---|---|---|---|---|
| | Gel conditions (%) | | Pure XG hydrogel | | $Cr^{3+}$ solution | | |
| Gel type | $m_x/m_w$ | Cr/XG | DI water | XG powder | DI water | $Cr(NO_3)_3 \cdot 9H_2O$ | NaCl |
| Pure XG hydrogel | 1.25 | 0 | 100 | 1.25 | — | — | — |
| | 2.5 | 0 | | 2.5 | — | — | — |
| | 5.0 | 0 | | 5.0 | — | — | — |
| XG–$Cr^{3+}$ gel | 1.25 | 15 | 100 | 2.5 | 100 | 0.375 | 0.25 |
| | 1.25 | 30 | | 2.5 | | 0.75 | 0.25 |
| | 1.25 | 60 | | 2.5 | | 1.5 | 0.25 |
| | 1.25 | 100 | | 2.5 | | 2.5 | 0.25 |
| | 2.5 | 15 | | 5.0 | | 0.75 | 0.5 |
| | 2.5 | 30 | | 5.0 | | 1.5 | 0.5 |
| | 2.5 | 60 | | 5.0 | | 3 | 0.5 |
| | 2.5 | 100 | | 5.0 | | 5 | 0.5 |
| | 5.0 | 15 | | 10.0 | | 1.5 | 1 |
| | 5.0 | 30 | | 10.0 | | 3 | 1 |
| | 5.0 | 60 | | 10.0 | | 6 | 1 |
| | 5.0 | 100 | | 10.0 | | 10 | 1 |

Note: $m_x/m_w$ (%) = mass ratio of XG powder to DI water; Cr/XG (%) = mass ratio of $Cr(NO_3)_3 \cdot 9H_2O$ to XG powder; and DI = deionized.

of the desired XG mass) was diluted in $Cr^{3+}$ solution to promote the efficient interaction between the XG and $Cr^{3+}$ by inducing XG molecules' repulsion (Pelletier et al. 2001).

Depending on the intended use, the XG–$Cr^{3+}$ gel or gel-treated soil was cured without evaporation after mixing. In this study, curing time refers to the period during which the gelation, in which the gel hardens as a result of polymerization via cation crosslinking, continues to progress with time without evaporation.

### Measurement of Yield Stress of XG–$Cr^{3+}$ Crosslinked Gel

In general, polymer-cation crosslinking affects the rheological properties of the crosslinked gel due to the formation of bonds between cations and functional groups of the polymer (Wang et al. 1994). The yield stress ($\tau_y$), one of the most important rheological properties of a structured fluid or gel, is the external stress necessary to initiate the flow of a fluid or disintegrate a gel structure (Jeong 2019). This study evaluated the gelation behavior of the crosslinked gel network in terms of $\tau_y$, taking into account the Cr/XG ratio, $m_x/m_w$, and the curing time, in accordance with the experimental protocol outlined next.

Rheometry was performed on pure XG and the XG–$Cr^{3+}$ gel using a rheometer (Rheolab QC, Anton Paar, Austria). For the evaluation of structured fluids, the vane cup system is superior to parallel-plate rheometry (Stokes and Telford 2004). The vane system consists of a cup (with a 29-mm inner diameter) and a four-blade vane spindle (width = 22 mm and height = 40 mm). The well-prepared pure XG and XG–$Cr^{3+}$ gels were immediately mounted in the cup and placed in the rheometer after mixing. The spindle was then carefully inserted until the vane was completely submerged in the gel.

To determine $\tau_y$, rotational shearing with a sufficiently low constant shear rate (i.e., 0.05 $s^{-1}$) was performed immediately or after a specific curing period (i.e., 1, 2, 6, 12, and 24 h) (Marudova-Zsivanovits et al. 2007). The torque response was collected at 2-s intervals for 600 s. As a result, the torque was measured, and Eq. (1) proposed by Dzuy and Boger (1985) was used to calculate the $\tau_y$ of XG and the XG–$Cr^{3+}$ gel

$$\tau_y = \frac{2}{\pi D^3}\left(\frac{H}{D}+\frac{1}{3}\right)^{-1} T_{\max} \tag{1}$$

where $\tau_y$ = yield stress (Pa); $D$ = vane width (m); $H$ = vane height (m); and $T_{max}$ = maximum torque (N·m).

Temperature was maintained at 25°C in the measuring system, and each test condition was performed three times to increase the validity of the results.

### Preparation of Pure XG and Crosslinked XG–$Cr^{3+}$-Treated Soil

After preparing pure XG and XG–$Cr^{3+}$ gels with $m_x/m_w = 1.25\%$, 2.50%, and 5%, the dried soil was uniformly mixed with the gel and molded. XG–$Cr^{3+}$ gel (Cr/XG = 0, 15, 30, 60, and 100%) was mixed with dried sand at $m_w/m_s = 20\%$, resulting in XG-to-soil contents in mass ratios ($m_x/m_s$) of 0.25%, 0.5%, and 1%, respectively, with an initial soil water content of 20%. All the XG–$Cr^{3+}$-treated soil samples were molded into a cubic shape (i.e., 40 × 40 × 40 mm) and cured in a mold according to the experiment's purpose and conditions (Table 2).

The strength of soils treated with XG–$Cr^{3+}$ was evaluated in terms of two moisture states: hydrated and dehydrated. The hydrated state indicates that the soil sample was preserved without

**Table 2.** UCS test conditions for XG–$Cr^{3+}$-treated soil

| | | Binder composition | | Specimen | |
|---|---|---|---|---|---|
| Purpose | Soil type | $m_x/m_s$ (%) | Cr/XG (%) | moisture state | Curing period |
| Strengthening | Sand | 0.25, 0.5, 1 | 0, 15, 30, 60, 100 | Wet | 1, 6, 12, 24, 48, 96, and 168 h curing without evaporation |
| | | | | Dry | Air-dehydration after 168 h cured |
| Long-term immersion durability | Sand | 1 | 0, 15, 30, 60, 100 | Wet | Immersed for 1, 3, 7, 14, 28, 50, and 100 days after 168 h of curing without evaporation |
| Cyclic wet–dry durability | Sand | 0.25, 0.5, 1 | 30 | Wet–dry | 24-h submerged and 48-h air-dehydration |

dehydration (evaporation), whereas the dehydrated state indicates that the soil sample was dried at 23°C until its weight remained constant.

### Unconfined Compressive Test for XG–$Cr^{3+}$-treated Soil

To evaluate the strength of the XG–$Cr^{3+}$-treated soil specimens, unconfined compressive strength (UCS) tests were conducted. The wet and dry UCS represent the measured strength under hydrated and dehydrated conditions. The wet UCS was evaluated after curing for 1, 6, 12, 24, 48, 96, and 168 h (or 0.04, 0.25, 0.5, 1, 2, and 7 days), whereas the dry UCS was evaluated after curing for 168 h and air-dehydration. The UCS test for XG–$Cr^{3+}$-treated soil was conducted in accordance with ASTM D2166 at a uniform loading rate of 1%/min using a master loader (HM-5030.3F, Humboldt, Illinois) (ASTM 2016). A three-sample mean was employed to represent each data point displayed in the obtained results.

### Microscopic Observation: Environmental Scanning Electron Microscopy

This study utilized an environmental scanning electron microscope (ESEM) (Quattro S, Thermo Fisher Scientific, Massachusetts) to examine the effect of dehydration on the microscale morphology of XG–$Cr^{3+}$-treated soil under humid-altered conditions (i.e., relative humidity from 100% to 0%). ESEM allowed for the regulation of the chamber's relative humidity by adjusting the water vapor pressure (Carrier et al. 2013). The relative humidity in the chamber decreased from 100% to 0% when XG–$Cr^{3+}$-treated sand ($m_x/m_s = 1\%$) was observed to simulate the dehydration process. In addition, air-dried XG–$Cr^{3+}$-treated sand ($m_x/m_s = 0.25\%$ and 1%) was observed in the vacuum state (relative humidity = 0%) to analyze the effect of $m_x/m_s$ on microscale morphology. During observation, each sample was affixed to a circular ESEM mount with carbon conductive adhesive, and the sample mount was exposed to the electron beams in the chamber.

### Durability Test for XG–$Cr^{3+}$-treated Soil

Durability of performance is one of the most concerning aspects of applying biopolymers in practical applications. This study tested the strength and durability of XG–$Cr^{3+}$-treated sand in two ways: long-term immersion and cyclic wetting–drying. XG–$Cr^{3+}$-treated sand cured for 7 days without dehydration was immersed in tap water for 1, 3, 7, 14, 28, 50, and 100 days for the long-term immersion test. After each period of immersion, the UCS was measured and compared with its initial strength.

For the cyclic wetting–drying test, XG–$Cr^{3+}$-treated sand samples were subjected to repeated cycles of wetting and drying, measuring UCS after each cycle in accordance with ASTM D559 (ASTM 2015). As an initial starting condition, the samples were cured for 7 days and then air-dehydrated for 2 weeks. Then, in one cycle, the samples were then immersed in water for 24 h (wetting phase) and dried for 48 h (drying phase). Six cycles of wetting–drying were conducted.

## Results and Analysis

### Effect of $Cr^{3+}$ Crosslinking on the Yield Stress of XG Hydrogel before Gelation

Under strain-controlled conditions, the yielding behaviors of XG–$Cr^{3+}$ gels ($m_x/m_w = 5\%$) with varying chromium contents (i.e., Cr/XG = 0%, 15%, 30%, 60%, and 100%) were investigated. The tests were performed within 10 min of mixing and setting thoroughly. As shown in Fig. 2(a), the torque value typically increased until the gel yielded and then declined; this indicates the gradual structural breakdown of the gel (James et al. 1987). With the addition of $Cr^{3+}$, both yield strain and peak torque value were increased, which involved mitigation of structural breakdown. The results of yield stress ($\tau_y$) of XG–$Cr^{3+}$ gel [Fig. 2(b)] showed that $\tau_y$ increased by a factor of 1.2–1.6 compared with pure XG (Cr/XG = 0%) with increases in Cr/XG. In addition, $\tau_y$ gradually increased, regardless of $m_x/m_w$, under identical Cr/XG conditions [Figs. 2(c and d)].

A highly concentrated XG solution exhibits low $\tau_y$ due to the XG polymers' tangled state (Song et al. 2006). Nonetheless, the increased $\tau_y$ after $Cr^{3+}$ addition at the initial state (i.e., curing period shorter than 10 min) could be attributed to the local interaction between $Cr^{3+}$ and the negatively charged side chain of the XG monomers during mixing and sample preparation. This conjugation between XG and $Cr^{3+}$ increases the effective macromolecule dimensions and molecular weight following network formation initiation (Ghoumrassi-Barr and Aliouche 2016; Marudova-Zsivanovits et al. 2007). Intriguingly, a higher XG concentration and $Cr^{3+}$ content were associated with a higher probability of simultaneous initiation, which resulted in a substantial increase in $\tau_y$ immediately after setting (Amir et al. 2019).

### Time-Dependent Gelation Behavior of XG–$Cr^{3+}$ Crosslinked Gel

The $\tau_y$ of the cured gel samples was measured to investigate the effect of curing time on gel strength. Fig. 3 depicts the torque-time response of XG–$Cr^{3+}$ gel under varying curing periods (0.1–24 h) with $m_x/m_w = 5\%$ and Cr/XG = 30%. During the curing period, the maximum torque value and modulus (initial slope of the curve) increased. Similar to typical observations for viscous biopolymer gel and bentonite suspensions, the torque increased gradually during the early stage of curing (0–2 h) and then plateaued with a higher yielding strain (Bekkour et al. 2005; Choi and Yoo 2009). These gradual gel structure breakdowns were likely induced by the rupture of the network bonds between the XG–$Cr^{3+}$ aggregates as a result of stretching (Choi and Yoo 2009).

As the curing period progressed beyond 2 h, both torque and slope increased drastically. At 6, 12, and 24 h, the torque increased linearly up to a peak value, exhibiting elastic–brittle behavior with significantly smaller yield strains. As the crosslinking-induced gelation progressed, the XG–$Cr^{3+}$ gels lost their viscoelasticity and became stiffer and more elastic, indicating that the failure mode was more similar to gel fracturing than flow initiation.

Fig. 4 depicts the time-dependent evolution of $\tau_y$ in an XG–$Cr^{3+}$ gel with varying $m_x/m_w$ and Cr/XG. During the gelation period, the $\tau_y$ of the XG–$Cr^{3+}$ gel ($m_x/m_w = 5\%$) developed a nonlinearly increasing trend, and a larger $\tau_y$ was observed at a higher Cr/XG ratio [Fig. 4(a)]. After 24 h curing, $\tau_y$ for the 15%, 30%, 60%, and 100% Cr/XG gels increased from 65, 76, 80, and 87 Pa to 1,300, 1,440, 1,610, and 1,610 Pa, respectively. In addition, the accumulation of $\tau_y$ in all conditions decreased at a rate proportional to the curing time.

According to Marudova-Zsivanovits et al. (2007), the gelation process of XG–$Cr^{3+}$ can be divided into three stages: latent (I), rising (II), and plateau (III) phases. During the latent period, the gel's rigidity is comparable to that of pure XG hydrogel. As gelation nears completion, the gel stiffens and demonstrates a significant increase in modulus during period (II), which converges to a plateau during period (III). Although crosslinking of XG–$Cr^{3+}$

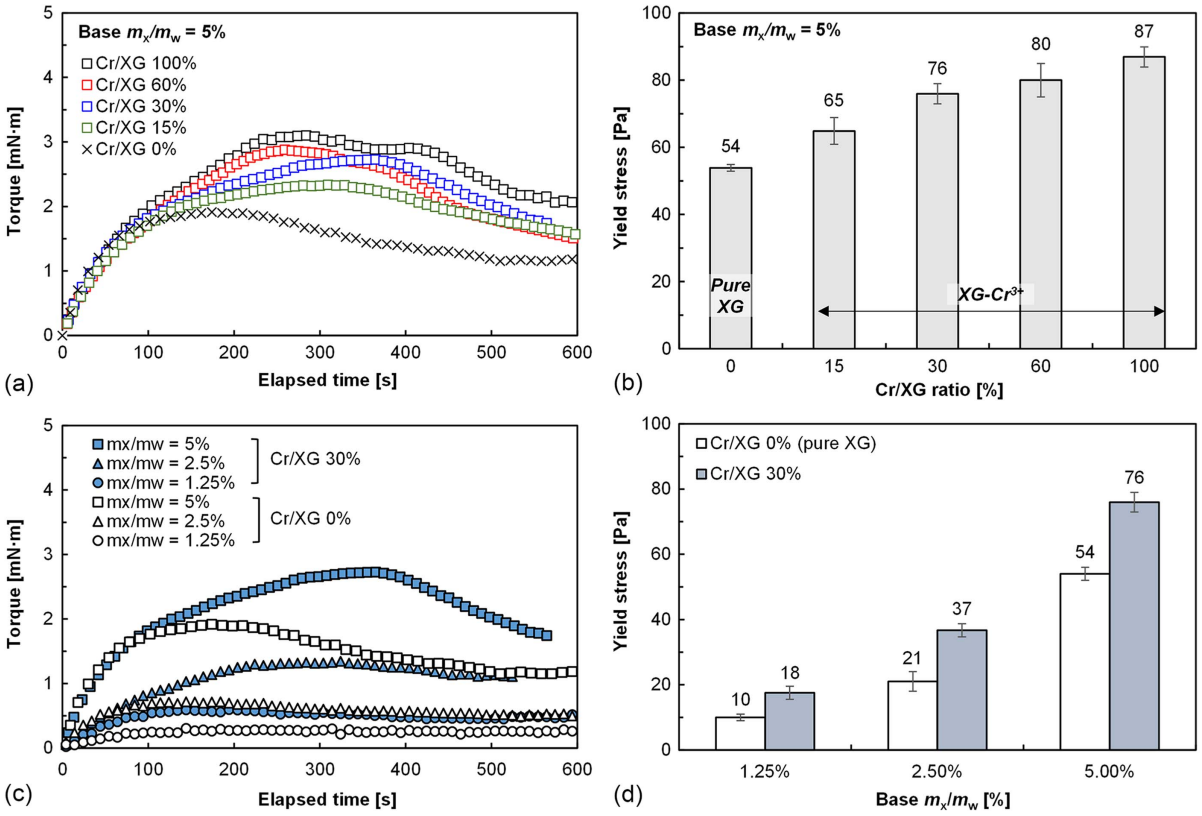


**Fig. 2.** Strain-controlled rheological characteristic of XG and XG–$Cr^{3+}$ hydrogel at initial state: (a) torque-time response with Cr/XG ratio; (b) yield stress variations with Cr/XG ratio; (c) torque-time response with $m_x/m_w$, and (d) yield stress variation with $m_x/m_w$.

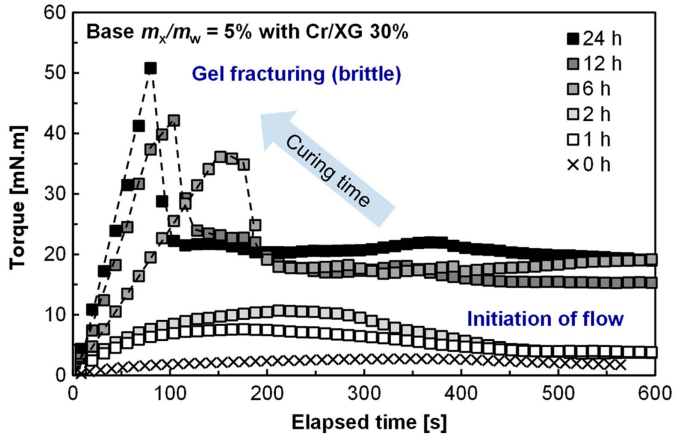


**Fig. 3.** Variation of torque–time response of XG–$Cr^{3+}$ hydrogel with curing period ($m_x/m_w = 5\%$ with $Cr/XG = 30\%$).

in this study was facilitated by using a significantly thicker XG hydrogel than in previous studies, the $\tau_y$ evolutions (1–24 h) in Fig. 4(a) correspond to a rising period (II). In addition, $\tau_y$ developed at a slower rate and will stagnate at the maximum gel strength.

The $\tau_y$ accumulation ($\Delta\tau_y$) up to 24 h was divided by four stages (0–2, 2–6, 6–12, and 12–24 h) and the amount of increment (as a percent ratio to total increment) at each stage is described in Fig. 4(b). The results demonstrated that the as Cr/XG increased, the $\tau_y$ rose faster and more dramatically, which is related to the frequency of the binding between $Cr^{3+}$ and XG increasing at the same time, resulting in a higher and faster gelation rate within 24 h (Marudova-Zsivanovits et al. 2007; Nolte et al. 1992). In accordance with Al-Muntasheri et al. (2007), the $m_x/m_w$ relating to the number of crosslinkable sites influences gelation rate more significantly [Figs. 4(c and d)]. As anticipated, a greater $m_x/m_w$ ratio increased the number of active carboxylate sites ($COO^-$), which frequently generated more three-dimensional, rigid gel networks through physical and ionic bonding with $Cr^{3+}$ cations (Amaral et al. 2021). Additionally, a higher $m_x/m_w$ ratio decreases the XG intermolecular distance, which increases the thickness of the XG–$Cr^{3+}$ network skeleton and widens the densely packed regions constituting the skeleton of the XG–$Cr^{3+}$ network, resulting in a stronger gel (Philippova et al. 2016).

Due to the fact that the XG–$Cr^{3+}$ gel strength increased significantly with the $m_x/m_w$ (i.e., base polymer concentration) or the $Cr^{3+}$ (i.e., crosslinker) to polymer ratio, the gelation could be accelerated to provide the possibility of a shorter gelation time for achieving the desired gel strength. This result is consistent with previous findings regarding the gelation properties of a crosslinked XG polymer gel with a diluted concentration (i.e., 0.05%–0.5% $m_x/m_w$) (Amir et al. 2019; Marudova-Zsivanovits et al. 2007).

### *Unconfined Compressive Strength of XG–$Cr^{3+}$-treated Soil*

Fig. 5(a) displays the stress–strain curve for the hydrated state XG–$Cr^{3+}$-treated sand sample (i.e., $m_x/m_s = 1\%$ with $Cr/XG = 15\%$–$100\%$) cured for 1 and 24 h as well as pure XG-treated samples (i.e., $Cr/XG = 0\%$). The ductile and weak behavior of pure XG-treated sand, with a low UCS of 10 kPa and a high failure strain

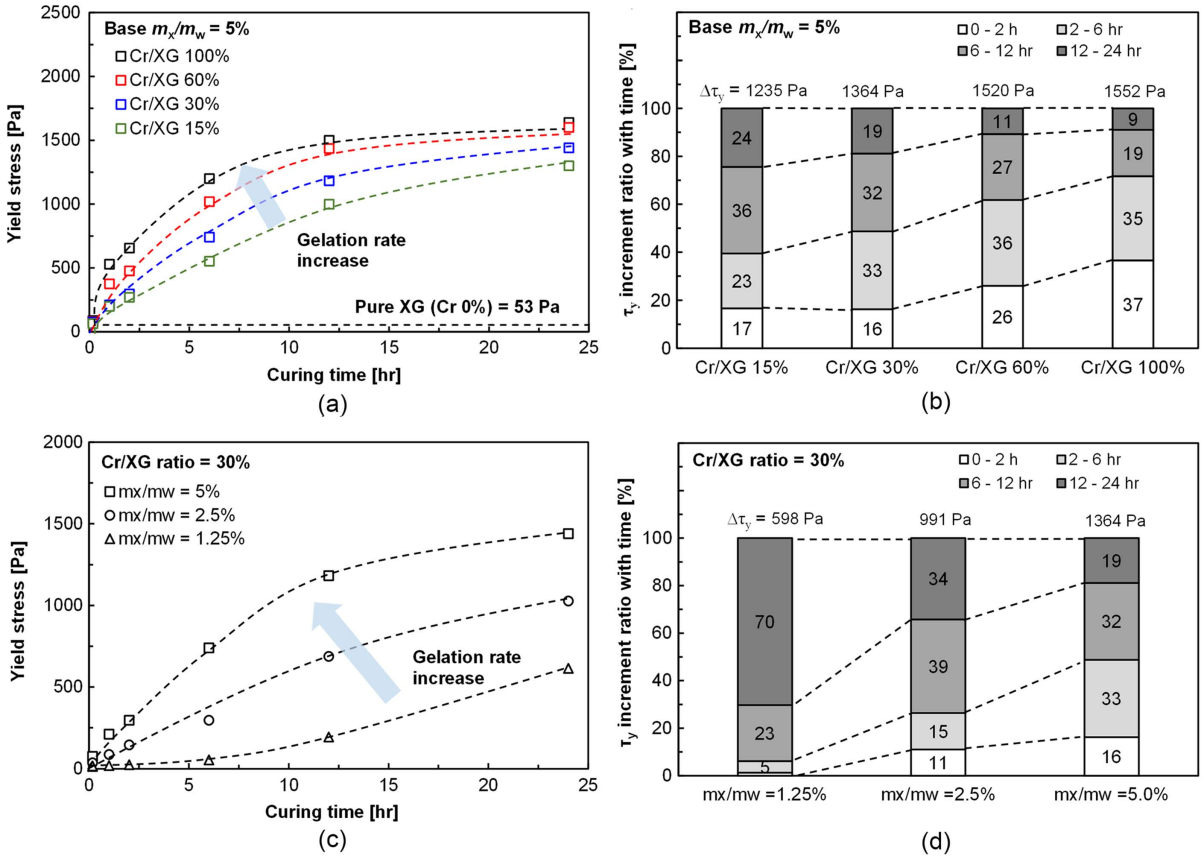


**Fig. 4.** Time-dependent yield stress development in XG–$Cr^{3+}$ crosslinked gel: (a) yield stress by curing time ($m_x/m_w = 5\%$); (b) increment percent of yield stress at each stage ($m_x/m_w = 5\%$); (c) yield stress by curing time (Cr/XG = 30%); and (d) increment percent of yield stress at each stage (Cr/XG = 30%).

of >10%, indicated that, despite its high viscosity, the pure XG hydrogel does not effectively strengthen the sand because there is no direct interaction between the XG molecules and the surface of the sand particles (Chang et al. 2015a). The $Cr^{3+}$-crosslinking modified the stress–strain curve of the XG-treated soil gradually in relation to curing period. After 1 h of curing (triangle mark), the peak compressive stress and failure strains increased slightly, indicating the onset of gelation. However, after 24 h of curing (rectangular mark), the peak compressive stress was significantly higher and the failure strain was lower (less ductile). This variation in the stress–strain curve was observed regardless of the varying $m_x/m_s$ ratios [Fig. 5(b)].

Furthermore, the time-dependent gelation of the XG–$Cr^{3+}$ treatment impacted the failure mode of the specimens under loading [Fig. 5(c)]. Although the specimen bulged with showing partial fissures in the lateral direction without prominently exhibiting any failure plane (at 1 h curing), the failure line could be distinguished with a wedge-shaped mode (i.e., double shear) as the curing period increased to 24 h. It denotes that the drastic rigidity development of the XG–$Cr^{3+}$ gel (in Fig. 3) occupying the sand pores predominantly altered the failure mode, and consequently XG–$Cr^{3+}$-treated sand stiffened and lost its ductility as gelation proceeded, thereby yielding a higher wet strength.

Fig. 6 depicts the UCS development over 7 days based on varying the Cr/XG ratio and $m_x/m_s$. The wet UCS of XG–$Cr^{3+}$-treated sand increased nonlinearly with curing time for a week, regardless of the Cr/XG ratio [Fig. 6(a)] and $m_x/m_s$ [Fig. 6(b)]. For instance, the UCS values of XG–$Cr^{3+}$-treated sand at $m_x/m_s = 1\%$ (Cr/XG = 15, 30, 60, and 100%) were increased about five to six times the initial UCS values (<50 kPa at 0.1 day elapsed).

Even after curing for 1 day, XG–$Cr^{3+}$-treated sand (i.e., $m_x/m_s = 1\%$ and Cr/XG = 100%) exhibited a significantly higher wet UCS (248 kPa) than gellan gum (187 kPa at 2% $m_{gellan}/m_s$) and malonic acid–crosslinked starch treatment (73 kPa at 6% $m_{starch}/m_s$) with identical sands that attempted to improve the wet strength by a heat-based process above 110°C (i.e., 383 K) (Chang et al. 2016a; Im et al. 2021). In addition, even a small amount of XG–$Cr^{3+}$ treatment ($m_x/m_s = 1\%$ with Cr/XG 30%) afforded a competitive 7-day UCS (450 kPa) when compared with cement-treated sand (380 kPa at $m_{cement}/m_s = 7\%$) (Cheng et al. 2013). As predicted by rheological tests, these results indicate that the low wet strength (i.e., 10 kPa at $m_x/m_s = 1\%$) of pure XG-treated sand could be significantly enhanced by XG–$Cr^{3+}$ crosslinking. Although pure XG and XG–$Cr^{3+}$ gel have fewer electrostatic interactions with the sand particles, the rigid gel structure surrounding the particles provides mechanical binding performance in soil.

Meanwhile, when cured for 7 days, the Cr/XG 15% and 30% conditions exhibited a higher wet UCS (~450 kPa) than the 60% (394 kPa) and 100% (360 kPa) conditions. This suggests that the higher the Cr/XG, the faster initial crosslinking occurs, and rapid strengthening (within a day) is possible; however, it can result in a smaller UCS due to less homogeneity in the gel matrix and syneresis (i.e., water extrusion and shrinkage) effects after a prolonged curing time (Di Lorenzo and Seiffert 2015; Jia et al. 2012; Zhang et al. 2017).

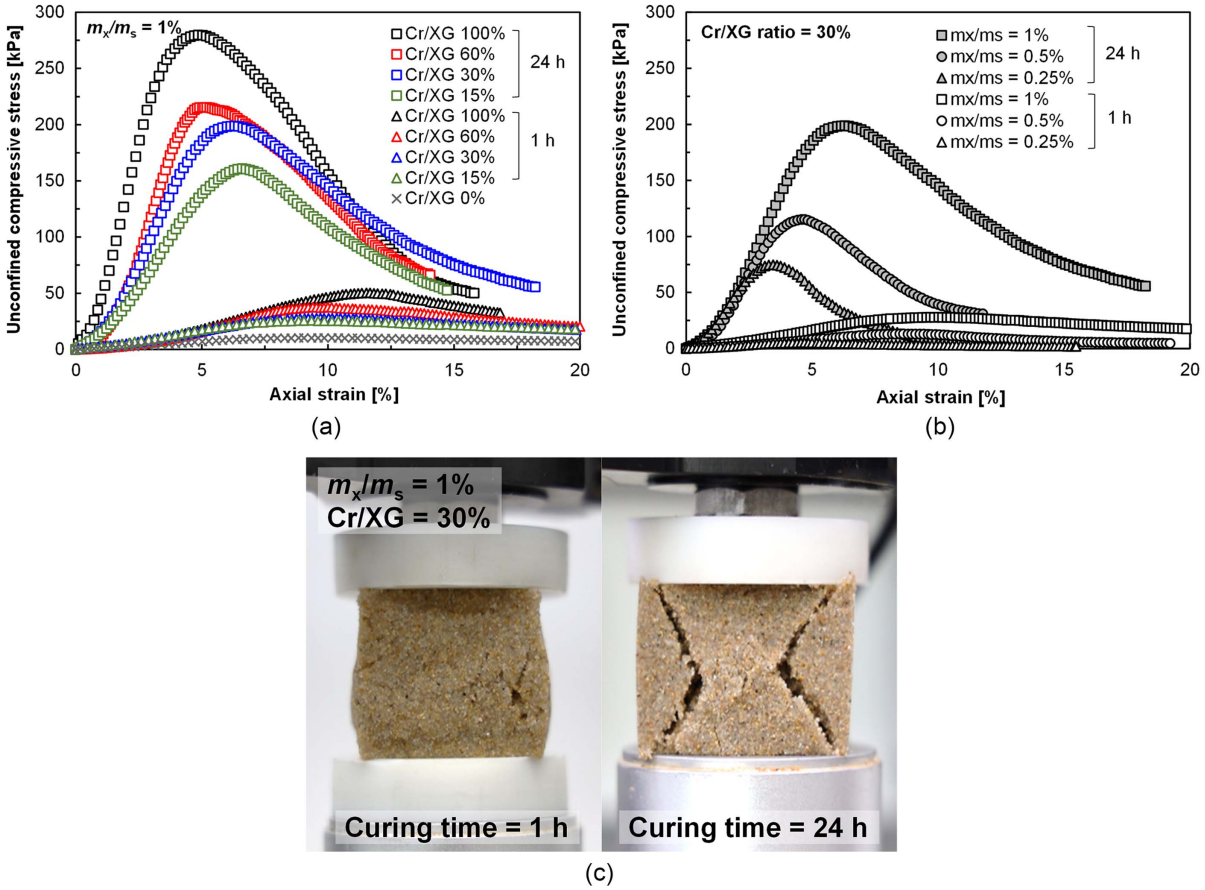


**Fig. 5.** Stress–strain relationship and failure mode of XG–$Cr^{3+}$-treated sand cured for 1 and 24 h: (a) effect of Cr/XG ratio (at $m_x/m_w = 1\%$); (b) effect of $m_x/m_s$ (at Cr/XG = 30%); and (c) failure mode at $m_x/m_w = 1\%$ and Cr/XG = 30%.

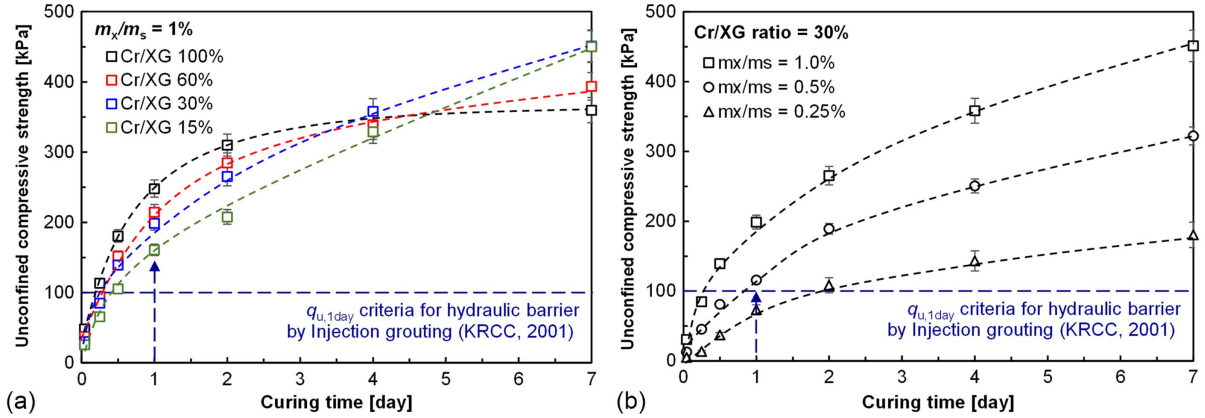


**Fig. 6.** Development of UCS with curing periods: effect of (a) Cr/XG ratio; and (b) $m_x/m_w$.

### *Dehydration Effect on Unconfined Compressive Strength of XG–$Cr^{3+}$-treated Soil*

Owing to the phase transition of XG from the viscous hydrogel to a tensile film, the XG treatment of soil demonstrates remarkably effective strengthening performance in dehydration condition (i.e., a higher UCS in a dry state) (Chang et al. 2015a). To investigate the effect of dehydration on the strength of XG–$Cr^{3+}$-treated soil, 7-day-cured specimens were dehydrated at room temperature for 2 weeks, and then assessed for UCS. All samples had final water contents less than 0.8%.

Fig. 7(a) depicts the changes in UCS of XG–$Cr^{3+}$-treated sand as a function of water content during the drying process. Regardless of Cr/XG, the UCS decreased linearly as soil samples were dried. Fig. 7(b) describes the representative stress–strain curve for the fully dried XG-treated sand and XG–$Cr^{3+}$-treated sand ($m_x/m_s = 1\%$). Compared with the responses in the hydrated state (Fig. 5), the axial stress and modulus of dehydrated pure XG-treated sand (Cr/XG = 0%) increased dramatically. In contrast, as the Cr/XG ratio increased, dehydrated XG–$Cr^{3+}$-treated sand exhibited a decrease in peak stress and failure strain.

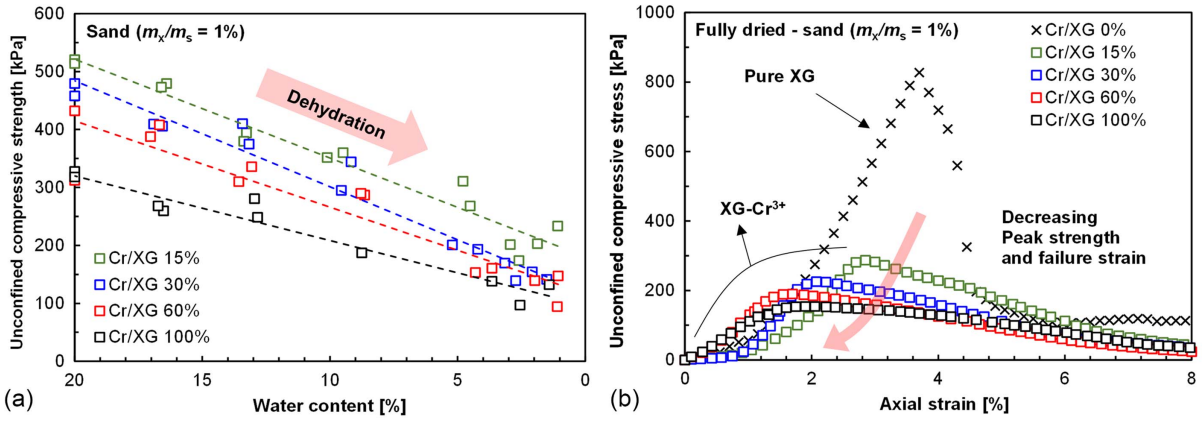


**Fig. 7.** Dehydration effect on UCS of XG–$Cr^{3+}$-treated sand: (a) UCS variation during dehydration process; and (b) stress–strain relationship of fully dried XG–$Cr^{3+}$-treated sand.

Fig. 8 compares the final dry UCS and initial wet UCS of XG–$Cr^{3+}$-treated soil with various Cr/XG and $m_x/m_s$. Although pure XG treatment in sand significantly increased the UCS from 10 to 830 kPa via dehydration, XG–$Cr^{3+}$ treatment decreased UCS by 51%–60% with different Cr/XG ratios [Fig. 8(a)], and the UCS degradation was more pronounced at a lower $m_x/m_s$ [Fig. 8(b)].

### ESEM Observation of XG–$Cr^{3+}$-Treated Soil

Although the electrostatically neutral sand grains do not interact with the XG molecules, dehydrated XG as a condensed biofilm facilitates mechanical bonding (i.e., interparticle cohesion) in cohesionless sand as well (Lee et al. 2021b). Therefore, the decrease in the dry UCS suggested that the crosslinking network between XG and $Cr^{3+}$ could prevent the formation of continuous mechanical bonding between the grains during dehydration. As depicted in Fig. 9, the ESEM observations were analyzed to determine the intergranular bonding characteristics of the XG–$Cr^{3+}$ gel.

Under the 100% relative humidity (wet state) condition, the XG–$Cr^{3+}$-treated sand ($m_x/m_s = 1\%$ and $Cr/XG = 30\%$) demonstrated that the sand grains were interconnected by the bulk and swollen gel [Fig. 9(a)]. As the sample was dehydrated by decreasing the relative humidity to zero, the bulk gel bridge experienced severe volumetric shrinkage, resulting in fissures at the intergranular bonding interface [Fig. 9(b)]. In addition, this volumetric shrinkage induced cracks on the film coating the particle surface [Fig. 9(c)] and accompanied the separation between the sand particles and XG–$Cr^{3+}$ film [Fig. 9(d)]. Thus, it can be confirmed that the loss of UCS and ductility of XG–$Cr^{3+}$-treated sand after dehydration is closely related to the deterioration of intergranular connectivity due to the severe shrinkage effect and the increase in brittleness in the dried gel itself due to crosslinking effect.

The $m_x/m_s$, on the other hand, affected the thickness of the dried XG–$Cr^{3+}$ gel matrix. At $m_x/m_s = 0.25\%$, a thin and highly fissured film was formed between the sand grains [Figs. 9(e and g)], whereas at $m_x/m_s = 1\%$, a relatively thick and highly condensed film was observed [Figs. 9(f and h)]. As the concentration of polymer decreased, the sand treated with XG–$Cr^{3+}$ became more vulnerable following dehydration.

### Strength Durability of XG–$Cr^{3+}$-Treated Soil against Water Exposure

Fig. 10 depicts the long-term immersion and cyclic wetting drying durability test results. One day after immersion, pure XG-treated sand samples were severely disturbed, with a high degree of dilution and surface swelling. In contrast, sand samples treated with XG–$Cr^{3+}$ remained unchanged for up to 100 days without swelling [Fig. 10(a)]. Due to the failure of the pure-XG-treated sand samples, they were excluded from subsequent evaluation. Fig. 10(b) depicts the UCS variations in XG–$Cr^{3+}$-treated sand ($m_x/m_s = 1\%$ with Cr/XG 15%–100%) during immersion. The UCS marginally increased during an immersion period of 100 days

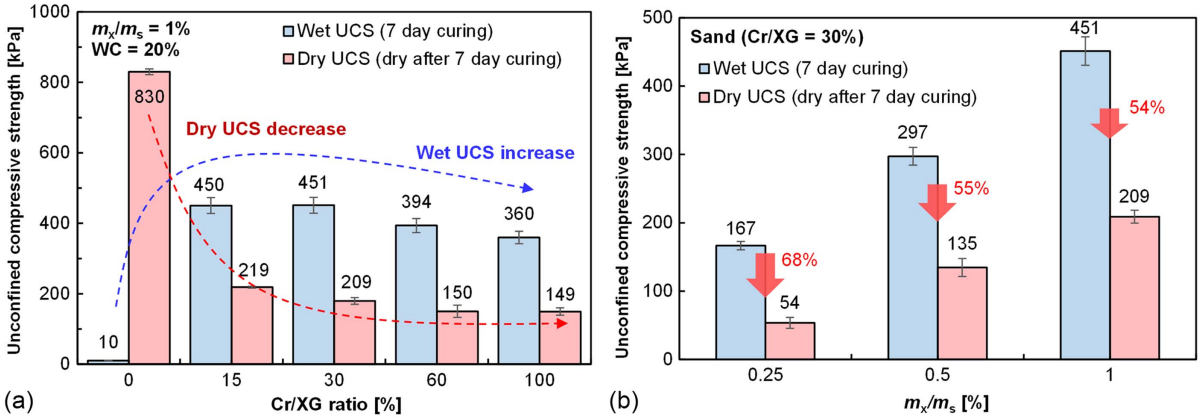


**Fig. 8.** Comparison between wet and dry UCS of XG–$Cr^{3+}$-treated soils with different (a) Cr/XG ratio; and (b) $m_x/m_s$.

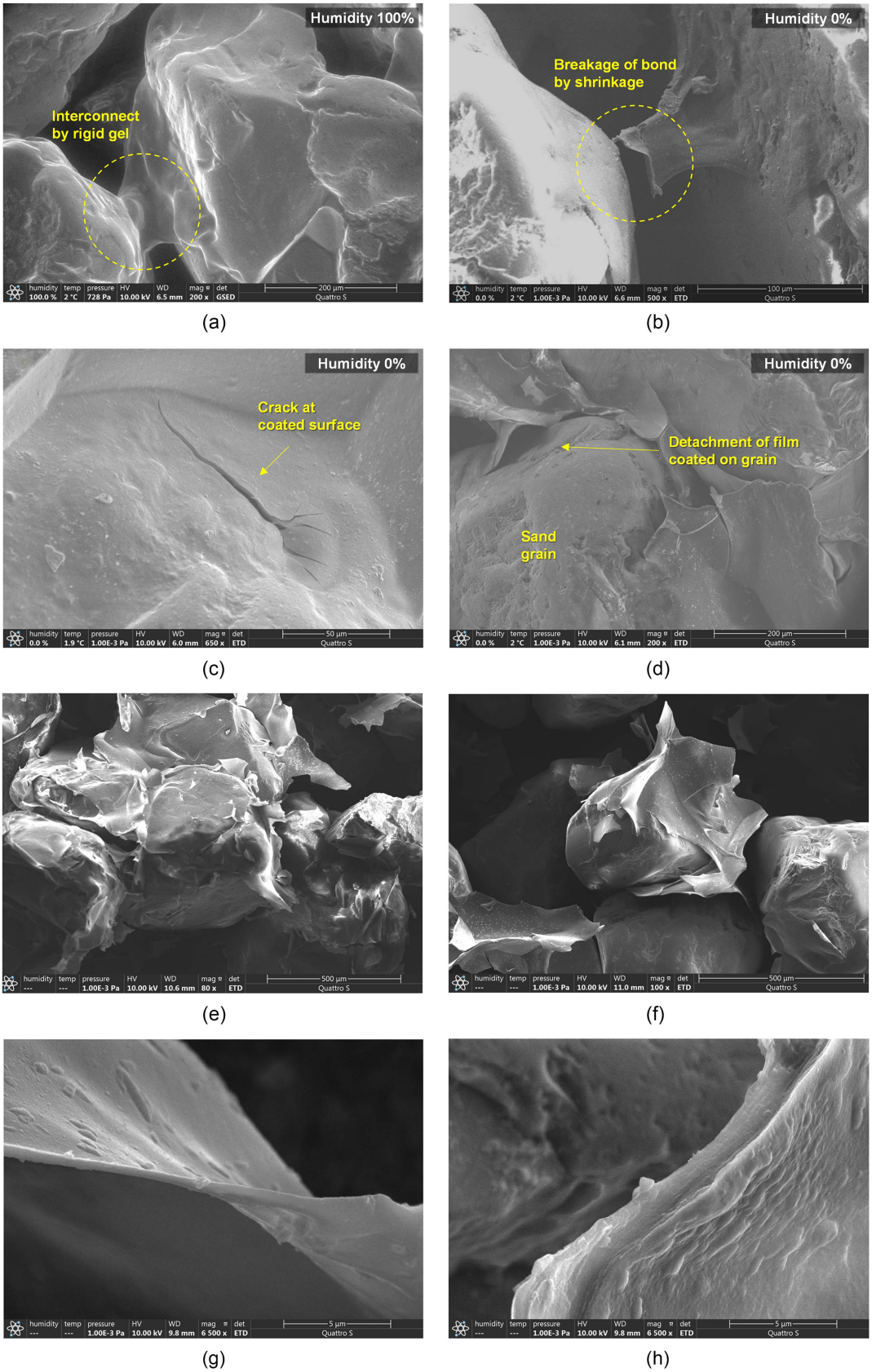


**Fig. 9.** ESEM images of XG–$Cr^{3+}$-treated sand ($m_x/m_s = 1\%$ and Cr/XG 30% condition): (a) intergranular gel bonding in humid state; (b) breakage of bonding in dried state; (c) cracks on film in dried state; (d) detachment of film in dried state; (e) XG–$Cr^{3+}$-treated sand of $m_x/m_w = 0.25\%$; (f) XG–$Cr^{3+}$-treated sand of $m_x/m_s = 1\%$; (g) XG–$Cr^{3+}$ film of $m_x/m_s = 0.25\%$; and (h) XG–$Cr^{3+}$ film of $m_x/m_s = 1\%$.

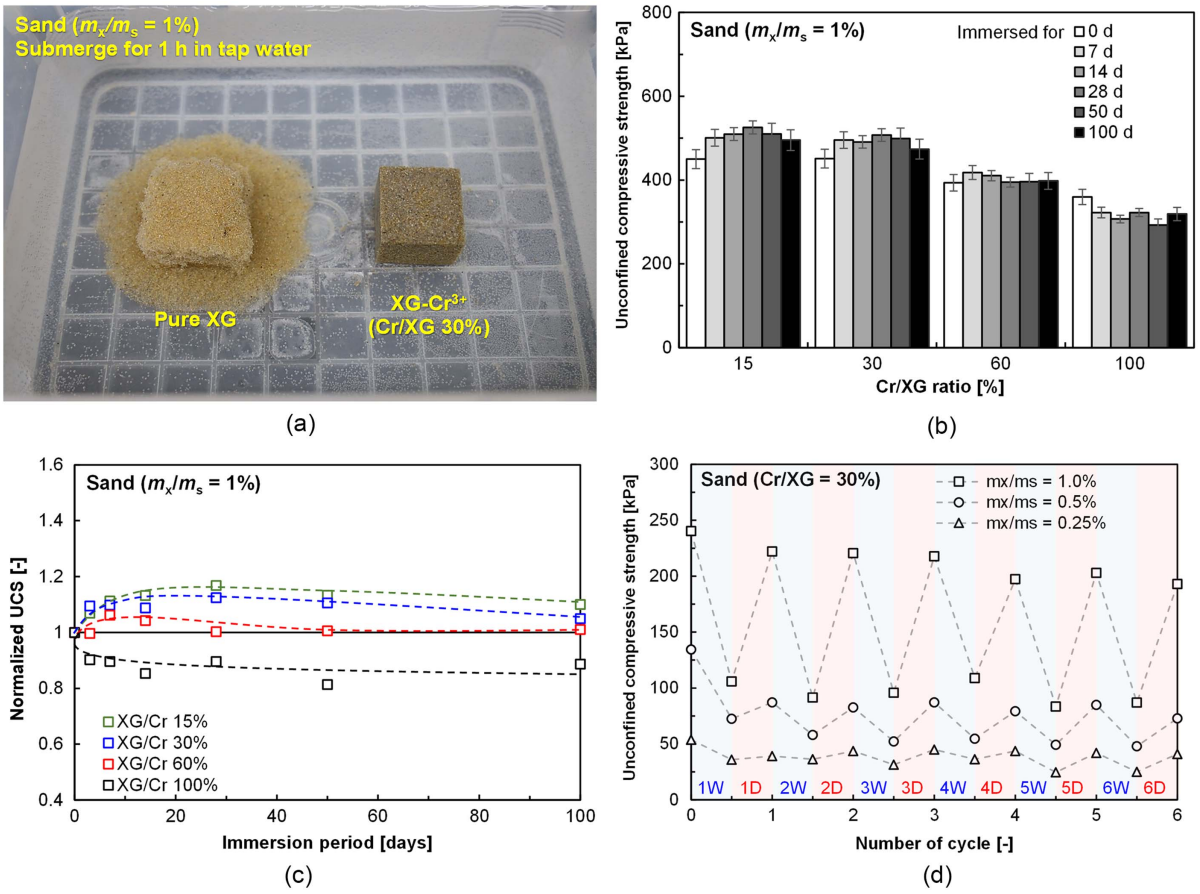


**Fig. 10.** Durability test results: (a) comparison between XG-treated and XG–$Cr^{3+}$-treated sand submerged for 1 h; (b) UCS variations during immersion; (c) normalized UCS variations under immersion period; and (d) UCS variations under cyclic wetting–drying process.

in the Cr/XG 15% (495 kPa) and Cr/XG 30% (473 kPa) conditions. For the Cr/XG 60% condition, UCS remained nearly constant (398 kPa); however, the UCS decreased from 360 to 319 kPa for the Cr/XG 100% condition. Fig. 10(c) presents the UCS normalized to the initial wet UCS obtained before immersion. After immersion for 100 days, the strength of Cr/XG 15% increased by 10%, whereas the UCS of Cr/XG 100% decreased by 12% relative to the initial condition.

Compared with the pure-XG-treated sand, which degraded rapidly, the results of the XG–$Cr^{3+}$-treated soil demonstrated that $Cr^{3+}$ crosslinking effectively reduced the water susceptibility of XG. Consumption of permissible carboxyl groups ($COO^-$) on the XG chain due to the covalent bonding with $Cr^{3+}$ reduced the water reactivity (Shibaev et al. 2020). Moreover, under saturated conditions, rigid XG–$Cr^{3+}$ network formation offers less reversibility. According to rheology tests, the gradual increase in strength under low Cr/XG conditions can be attributed to the relatively slower gelation speed. However, the decrease in strength at a high Cr/XG ratio is presumed to be caused by syneresis of the XG–$Cr^{3+}$ gel. Under conditions of extremely high $Cr^{3+}$ concentrations, the syneresis characteristics of the crosslinked gel were typically observed (Gales et al. 1994), and early onset of syneresis occurs during over-crosslinking (Pereira et al. 2022; Zhang et al. 2015). Consequently, a high Cr/XG (e.g., Cr/XG = 100%) may have negative effect on the strength durability under resaturation, despite its rapid strengthening efficiency.

The response of the UCS to the cyclic wet–dry process [Fig. 10(d)] showed that XG–$Cr^{3+}$-treated sand maintained 76%–80% of initial dry UCS after six cycles, in contrast to the pure XG-treated sand sample, which was completely degraded after only the first wetting in the study by Lee et al. (2022). Particularly, the dry UCS decreased after 24-h submerge (wetting phase) due to slight water absorption; however, once XG–$Cr^{3+}$ gel is dried, the film does not revert into the rigid or viscoelastic hydrogel phase as before.

## Discussion

### *Strength and Durability Enhancement of XG-Treated Soil via $Cr^{3+}$ Crosslink–Induced Gelation*

Fig. 11 summarize the strength results with conceptual microstructure model of XG and XG–$Cr^{3+}$-treated sand in hydrated (initially wet) and dehydrated condition. The results obtained under various conditions confirmed that the gelation of XG–$Cr^{3+}$ crosslinking significantly improves the wet UCS in sandy soil. In addition, the development of crosslinked gel strength (yield stress, $\tau_y$) and wet UCS in soil was accelerated under both conditions of higher XG polymer concentration and $Cr^{3+}$ amounts.

The gelation resulting from the reaction between $Cr^{3+}$ and the XG chain can be explained by three types of linkage: (1) intermolecular crosslinks, (2) intramolecular crosslinks, and (3) $Cr^{3+}$ bound to individual polymer chains (Gales et al. 1994). Among these linkages, the intermolecular crosslink associated with the formation of a gel's backbone restricts the deformation of the

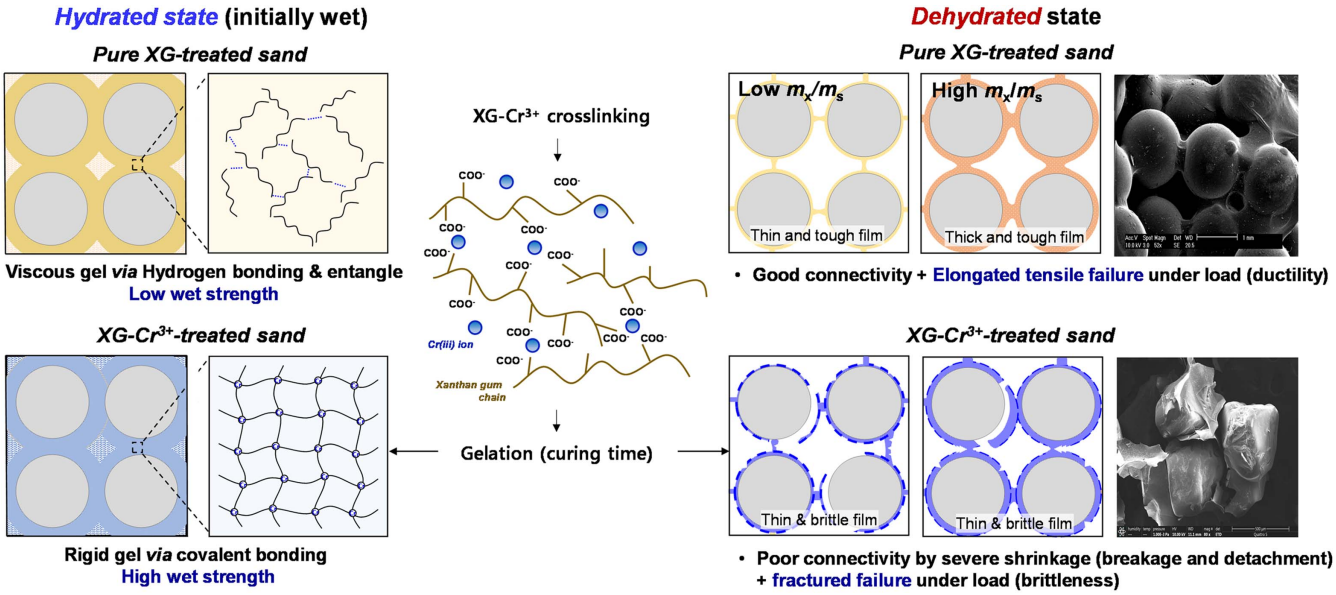


**Fig. 11.** Schematic model of microstructure of XG-treated sand, XG–$Cr^{3+}$gel, and XG–$Cr^{3+}$-treated sand.

XG–$Cr^{3+}$ network, thereby contributing to the network's overall strength. Consequently, an increase in the number of active sites (carboxyl groups) increases the likelihood of an intermolecular reaction, which facilitates the attainment of greater strength. Moreover, $m_x/m_w$ dominantly influences the overall strength of the XG–$Cr^{3+}$ gel and treated sand more than the amount of $Cr^{3+}$.

The significant decrease in reactivity between water molecules and XG polymer after gelation can rationalized on the basis of the consumption of $COO^-$ and varying bonding strength. Due to the consumption of $COO^-$ during XG–$Cr^{3+}$ crosslinking via the aforementioned three mechanisms, fewer water molecules can reinteract with XG chains. In addition, the difference in bonding strength between the covalent bonds with $Cr^{3+}$ and the hydrogen bonds with water contributes to the suppression of water reactivity (Jeffrey and Saenger 2012). These characteristics adequately validate the conclusion that the addition of $Cr^{3+}$ to XG-treated sand significantly increases its durability under submerged conditions.

However, soil reinforcement via XG–$Cr^{3+}$ gelation is only possible in the presence of a minimum amount of XG and an adequate amount of $Cr^{3+}$. In the case of using excessively diluted XG, the increased distance between the XG polymer chains reduces the probability of intermolecular crosslinking drastically. Similarly, if an insufficient amount of $Cr^{3+}$ is introduced, crosslinking generates sols rather than a bulk rigid gel. In the event that an excessive amount of $Cr^{3+}$ is added, the gel can be degraded by syneresis as the water is expelled from the gel via osmosis; this dehydrates the polymer gel (Gales et al. 1994). Therefore, the optimal usage amount must be determined based on the required target strength and gel time for effective soil reinforcement. In addition, depending on the pH and temperature, XG molecules typically undergo conformational change from a double helical form to a coiled form in a disordered state, which may result in a distinct binding pattern and mechanical strength after crosslinkage; therefore, this aspect of XG should be investigated further in future research.

### *Potential Applications of XG–$Cr^{3+}$ Soil Treatment in Geotechnical Engineering Practices*

Prior research has investigated the viability of XG treatment in injection grouting (i.e., as a temporary hydraulic barrier) due to its shear-thinning property, which facilitates penetration. Due to the high viscosity and swelling properties of XG, the injection of the XG hydrogel may prevent water infiltration into the soil media or adjacent soil–structure interface (Lee et al. 2021a). However, concerns exist regarding the XG treatment's insufficient strength in the hydrated state and washout issues under high-water-pressure conditions.

The present experimental findings confirmed that the gelation of XG–$Cr^{3+}$ enhanced the strength of coarse soil in a hydrated state without the need for heat or pH regulation. In addition, the results demonstrated that the strength can be maintained under a saturated condition for an extended period of time due to the decreased water reactivity. In practical applications, therefore, the $Cr^{3+}$-induced crosslinking method can increase the potential of XG soil treatment.

Fig. 12 compares the wet UCS of XG–$Cr^{3+}$-treated sand, cement-treated sand (Park 2011), and other previously attempted biopolymer treatments for soil reinforcement: $\beta$-glucan (Chang and Cho 2012), gellan gum (Chang et al. 2017), agar gum (Chang et al. 2015b), and starch (Im et al. 2021). The results indicate that XG–$Cr^{3+}$ ($m_x/m_s = 1\%$ and $Cr/XG = 30\%$) significantly increased the UCS in a hydrated condition (i.e., 450 kPa), which is roughly three times that of the 2% cement-treated sand (i.e., 155 kPa). In addition, the XG–$Cr^{3+}$-treated soil samples were

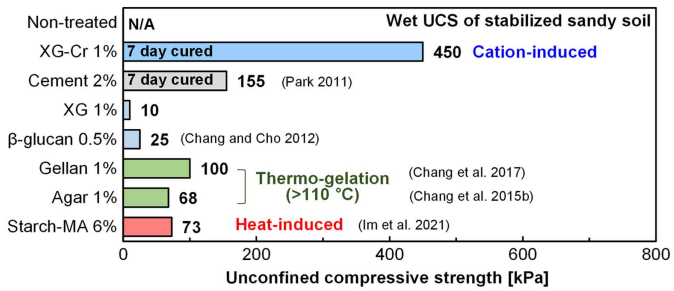


**Fig. 12.** UCS of XG–$Cr^{3+}$-treated soil compared with cement-treated and various biopolymer-treated soils. (Data from Park 2011; Chang and Cho 2012; Chang et al. 2017, 2015b; Im et al. 2021.)

four to six times stronger than those treated with thermogelation biopolymers (e.g., gellan and agar gum) and heat-induced crosslinked biopolymer (e.g., starch-malonic acid composite), which require sufficient heating temperatures above 110°C (i.e., 383 K).

Furthermore, one of the benefits of XG–$Cr^{3+}$ crosslinking is its ability to control the gelation period, whereas $Ca^{2+}$- or $Al^{3+}$-induced cross-linkages occur almost instantaneously (Farrés and Norton 2014; Rahbari and Francois 1992). Adjusting the mixing recipes permits the achievement of high wet strength within the required time. As depicted in Fig. 6, XG–$Cr^{3+}$ treatment in sand can achieve a strength greater than 200 kPa in less than 24 h, thereby satisfying the UCS requirement in a single day ($q_{u,1\ \mathrm{day}}$) for the curtain grouting method recommended by the dam and embankment design criteria of South Korea (KRCC 2001). Therefore, XG–$Cr^{3+}$ treatment is practically applicable for time-controllable ground reinforcement.

Through $Cr^{3+}$ crosslinking, the applicability of the proposed method for injection grouting can be expanded. In general, the post-stability (i.e., washout resistance) in terms of the hydraulic pressure gradient, which is the minimum pressure gradient required to drain the grout, is closely related to the grout's static yield stress ($\tau_y$). Based on the current finding that demonstrated a 25-fold increase in the $\tau_y$ of XG (from 53 to 1,300 Pa) within a single day by adding 15% $Cr^{3+}$ to XG (Fig. 4), it is anticipated that the pressure gradient resistance of XG gel will also increase significantly.

However, the increase in $\tau_y$ during the mixing stage and application period may impede the injectability (i.e., soil media penetration) of the XG–$Cr^{3+}$ gel (Axelsson et al. 2009). As the initial $\tau_y$ and subsequent gel time can be modified by adjusting $m_x/m_w$ and Cr/XG, the optimal recipe for the intended application must be determined. Consequently, $Cr^{3+}$ crosslinking can be considered an effective method for enhancing the viability of XG injection in high-water-pressure conditions for hydraulic barriers.

Consideration must also be given to the environmental impact for future field application. Because $Cr^{3+}$ is a naturally derived element involved in the human metabolism, it is known that be less toxic and less soluble than hexavalent chromium ($Cr^{6+}$) (Preuss and Anderson 1998). According to Eary and Rai (1987), inorganic oxidation of $Cr^{3+}$ to $Cr^{6+}$ occurs rarely in soil or waste, with the exception of oxidation by manganese oxides. Moreover, although aerobic oxidation of $Cr^{3+}$ to $Cr^{6+}$ is thermodynamically possible, it requires a high temperature (200°C–300°C); consequently, this reaction extremely rare in aquatic environments (Apte et al. 2006; Gorny et al. 2016). However, further research should be conducted on the environmental impact and potential leaching effect of $Cr^{3+}$ under practical onsite conditions.

## Conclusions

To overcome the low strength efficiency and water-durability of XG-treated soil in a hydrated state, XG–$Cr^{3+}$ crosslinking was adopted for XG-treated soil to enhance the UCS at the initially wet state and even after long-term water exposure. The exploration of rheology led to an in-depth comprehension of the gel formation behavior and consequent gel strength development as a function of $m_x/m_w$ and Cr/XG. In addition, a series of UCS and durability tests demonstrated that $Cr^{3+}$ crosslinking can effectively assist soil binding and strengthening in a hydrated state, and increase the feasibility of XG-soil treatment in field applications. In summary, the following conclusions could be drawn:

- The addition of $Cr^{3+}$ to XG hydrogel induced a slight increase in $\tau_y$ at the initial state. As the crosslinking-induced gelation progressed, XG–$Cr^{3+}$ gel lost its viscoelasticity and became stiffer (elastic-brittle behavior), exhibiting a failure mode similar to gel fracture. The rigid gel network formed by gradual intermolecular aggregation via covalent bonding between $Cr^{3+}$ and carboxyl groups of XG polymer chains is primary mechanism responsible for the time-dependent development of XG–$Cr^{3+}$ gel strength. The gel strength and gelation rate can be altered by adjusting XG and $Cr^{3+}$ concentrations.
- The UCS tests confirmed that the gelation of XG–$Cr^{3+}$ increased the strength of coarse soil in a hydrated state without requiring heat or pH regulation. XG–$Cr^{3+}$ treatment in sand can achieve a strength greater than 200 kPa within a day, which satisfies the requirement for curtain grouting. In addition, XG–$Cr^{3+}$-treated sand exhibited competitive $q_{u,7\ \mathrm{day}}$ (450 kPa) to cement-treated, thermogelated biopolymer–treated, and heat-induced crosslinked biopolymer–treated sands at a comparable dosage.
- The consumption of the hydrophilic site in the XG chains by crosslinking decreased the water susceptibility after gelation and, as a result, increased the strength durability under prolonged immersion. Under 100 days of immersion, XG–$Cr^{3+}$-treated sand with a Cr/XG ratio of 15%–30% exhibited excellent UCS stability, whereas sand with a Cr/XG ratio of 60%–100% degraded gradually by syneresis.
- As opposed to pure XG-treated sand, $Cr^{3+}$ crosslinking resulted in a lower dry UCS after the dehydration process. Under loading, pure XG gel exhibited good connectivity and elongated tensile failure, whereas XG–$Cr^{3+}$ gel displayed poor connectivity, severe shrinkage, and brittle failure. Once XG–$Cr^{3+}$ gel is dried, the XG–$Cr^{3+}$ film does not revert into the rigid or viscoelastic hydrogel phase as before.
- XG–$Cr^{3+}$ gel and XG–$Cr^{3+}$ soil treatment can be employed as a strength/time-controllable grout material in geotechnical engineering applications requiring rapid strengthening. It could be injected into the interior of waterfront soil embankments and soil–structure interfaces to effectively prevent groundwater infiltration and increase bearing capacity. However, the shear behavior, hydraulic performance, and environmental impact of XG–$Cr^{3+}$-treated soils should be validated in further.

## Data Availability Statement

All data, models, and code generated or used during the study appear in the published article.

## Acknowledgments

This research was supported by the National Research Foundation of Korea (NRF) grant funded by the Korean government (MSIT) (Nos. 2017R1A5A1014883 and 2022R1A2C2091517).

Author contributions: Minhyeong Lee contributed to the conceptualization, methodology, investigation, data curation, visualization, validation, and writing the original draft. Ilhan Chang contributed to the validation, writing—review and editing, visualization, and supervision. Gye-Chun Cho contributed to the resources, supervision, project administration, and funding acquisition.

## Notation

*The following symbols are used in this paper:*

$C_c$ = coefficient of curvature;

$C_u$ = coefficient of uniformity;

Cr/XG = chromium nitrate-to-XG mass ratio (%);
$D$ = width of vane (m);
$D_{50}$ = mean particle size (mm);
$e_{max}$ = maximum void ratio;
$e_{min}$ = minimum void ratio;
$G_s$ = specific gravity;
$H$ = height of vane (m);
LL = liquid limit (%);
$m_{cement}/m_s$ = cement-to-soil mass ratio (%);
$m_{gellan}/m_s$ = gellan gum-to-soil mass ratio (%);
$m_{starch}/m_s$ = starch-to-soil mass ratio (%);
$m_w/m_s$ = water-to-soil mass ratio (%);
$m_x/m_s$ = XG-to-soil mass ratio (%);
$m_x/m_w$ = XG-to-water mass ratio (%);
PL = plastic limit (%);
$q_{u,1\ day}$ = 1-day UCS (kPa); and
$q_{u,7\ day}$ = 7-day UCS (kPa).

## References


Ahmad, N. H., S. Mustafa, and Y. B. Che Man. 2015. "Microbial polysaccharides and their modification approaches: A review." *Int. J. Food Prop.* 18 (2): 332–347. https://doi.org/10.1080/10942912.2012.693561.

Al-Muntasheri, G. A., H. A. Nasr-El-Din, and I. A. Hussein. 2007. "A rheological investigation of a high temperature organic gel used for water shut-off treatments." *J. Pet. Sci. Eng.* 59 (1–2): 73–83. https://doi.org/10.1016/j.petrol.2007.02.010.

Alvarez-Lorenzo, C., B. Blanco-Fernandez, A. M. Puga, and A. Concheiro. 2013. "Crosslinked ionic polysaccharides for stimuli-sensitive drug delivery." *Adv. Drug Delivery Rev.* 65 (9): 1148–1171. https://doi.org/10.1016/j.addr.2013.04.016.

Amaral, C. N., P. F. Oliveira, L. G. Pedroni, and C. R. Mansur. 2021. "Viscoelastic behavior of hydrogel-based xanthan gum/aluminum lactate with potential applicability for conformance control." *J. Appl. Polym. Sci.* 138 (27): 50640. https://doi.org/10.1002/app.50640.

Amir, Z., I. M. Said, and B. M. Jan. 2019. "In situ organically cross-linked polymer gel for high-temperature reservoir conformance control: A review." *Polym. Adv. Technol.* 30 (1): 13–39. https://doi.org/10.1002/pat.4455.

Apte, A. D., V. Tare, and P. Bose. 2006. "Extent of oxidation of Cr (III) to Cr (VI) under various conditions pertaining to natural environment." *J. Hazard. Mater.* 128 (2–3): 164–174. https://doi.org/10.1016/j.jhazmat.2005.07.057.

Argin, S., P. Kofinas, and Y. M. Lo. 2014. "The cell release kinetics and the swelling behavior of physically crosslinked xanthan–chitosan hydrogels in simulated gastrointestinal conditions." *Food Hydrocolloids* 40 (Oct): 138–144. https://doi.org/10.1016/j.foodhyd.2014.02.018.

ASTM. 2015. *Standard test methods for wetting and drying compacted soil-cement mixtures*. ASTM D559/D559M-15. West Conshohocken, PA: ASTM.

ASTM. 2016. *Standard test method for unconfined compressive strength of cohesive soil*. ASTM D2166/D2166M-16. West Conshohocken, PA: ASTM.

ASTM. 2020. *Standard test method for particle size distribution of catalytic materials by laser light scattering*. ASTM D4464-15. West Conshohocken, PA: ASTM.

Avery, M., L. Burkholder, and M. Gruenenfelder. 1986. "Use of crosslinked xanthan gels in actual profile modification field projects." In *Proc., Int. Meeting on Petroleum Engineering*. Beijing: OnePetro.

Axelsson, M., G. Gustafson, and Å. Fransson. 2009. "Stop mechanism for cementitious grouts at different water-to-cement ratios." *Tunnelling Underground Space Technol.* 24 (4): 390–397. https://doi.org/10.1016/j.tust.2008.11.001.

Ayeldeen, M. K., A. M. Negm, and M. A. El Sawwaf. 2016. "Evaluating the physical characteristics of biopolymer/soil mixtures." *Arabian J. Geosci.* 9 (5): 1–13. https://doi.org/10.1007/s12517-016-2366-1.

Baruthio, F. 1992. "Toxic effects of chromium and its compounds." *Biol. Trace Elem. Res.* 32 (1): 145–153. https://doi.org/10.1007/BF02784599.

Bekkour, K., M. Leyama, A. Benchabane, and O. Scrivener. 2005. "Time-dependent rheological behavior of bentonite suspensions: An experimental study." *J. Rheol.* 49 (6): 1329–1345. https://doi.org/10.1122/1.2079267.

Butler, M. 2016. *Xanthan Gum: Applications and research studies*. New York: Nova Science.

Cabalar, A., M. Wiszniewski, and Z. Skutnik. 2017. "Effects of xanthan gum biopolymer on the permeability, odometer, unconfined compressive and triaxial shear behavior of a sand." *Soil Mech. Found. Eng.* 54 (5): 356–361. https://doi.org/10.1007/s11204-017-9481-1.

Cabalar, A. F., and H. Canakci. 2011. "Direct shear tests on sand treated with xanthan gum." *Proc. Inst. Civ. Eng. Ground Improv.* 164 (2): 57–64. https://doi.org/10.1680/grim.800041.

Carrier, B., L. Wang, M. Vandamme, R. J. M. Pellenq, M. Bornert, A. Tanguy, and H. Van Damme. 2013. "ESEM study of the humidity-induced swelling of clay film." *Langmuir* 29 (41): 12823–12833. https://doi.org/10.1021/la402781p.

Casas, J. A., V. E. Santos, and F. García-Ochoa. 2000. "Xanthan gum production under several operational conditions: Molecular structure and rheological properties." *Enzyme Microb. Technol.* 26 (2): 282–291. https://doi.org/10.1016/S0141-0229(99)00160-X.

Chang, I., and G.-C. Cho. 2012. "Strengthening of Korean residual soil with $\beta$-1,3/1,6-glucan biopolymer." *Constr. Build. Mater.* 30 (May): 30–35. https://doi.org/10.1016/j.conbuildmat.2011.11.030.

Chang, I., J. Im, and G.-C. Cho. 2016a. "Geotechnical engineering behaviors of gellan gum biopolymer treated sand." *Can. Geotech. J.* 53 (10): 1658–1670. https://doi.org/10.1139/cgj-2015-0475.

Chang, I., J. Im, and G.-C. Cho. 2016b. "Introduction of microbial biopolymers in soil treatment for future environmentally-friendly and sustainable geotechnical engineering." *Sustainability* 8 (3): 251. https://doi.org/10.3390/su8030251.

Chang, I., J. Im, S.-W. Lee, and G.-C. Cho. 2017. "Strength durability of gellan gum biopolymer-treated Korean sand with cyclic wetting and drying." *Constr. Build. Mater.* 143 (Jul): 210–221. https://doi.org/10.1016/j.conbuildmat.2017.02.061.

Chang, I., J. Im, A. K. Prasidhi, and G.-C. Cho. 2015a. "Effects of xanthan gum biopolymer on soil strengthening." *Constr. Build. Mater.* 74 (Jan): 65–72. https://doi.org/10.1016/j.conbuildmat.2014.10.026.

Chang, I., Y.-M. Kwon, and G.-C. Cho. 2021. "Effect of pore–fluid chemistry on the undrained shear strength of xanthan gum biopolymer-treated clays." *J. Geotech. Geoenviron. Eng.* 147 (11): 06021013. https://doi.org/10.1061/(ASCE)GT.1943-5606.0002652.

Chang, I., M. Lee, and G.-C. Cho. 2019. "Global CO2 emission-related geotechnical engineering hazards and the mission for sustainable geotechnical engineering." *Energies* 12 (13): 2567. https://doi.org/10.3390/en12132567.

Chang, I., M. Lee, A. T. P. Tran, S. Lee, Y.-M. Kwon, J. Im, and G.-C. Cho. 2020. "Review on biopolymer-based soil treatment (BPST) technology in geotechnical engineering practices." *Trans. Geotech.* 24 (Sep): 100385. https://doi.org/10.1016/j.trgeo.2020.100385.

Chang, I., A. K. Prasidhi, J. Im, and G.-C. Cho. 2015b. "Soil strengthening using thermo-gelation biopolymers." *Constr. Build. Mater.* 77 (Feb): 430–438. https://doi.org/10.1016/j.conbuildmat.2014.12.116.

Chang, I., A. K. Prasidhi, J. Im, H.-D. Shin, and G.-C. Cho. 2015c. "Soil treatment using microbial biopolymers for anti-desertification purposes." *Geoderma* 253–254 (Sep): 39–47. https://doi.org/10.1016/j.geoderma.2015.04.006.

Chen, C., L. Wu, and M. Harbottle. 2019. "Exploring the effect of biopolymers in near-surface soils using xanthan gum–modified sand under shear." *Can. Geotech. J.* 57 (8): 1109–1118. https://doi.org/10.1139/cgj-2019-0284.

Cheng, L., R. Cord-Ruwisch, and M. A. Shahin. 2013. "Cementation of sand soil by microbially induced calcite precipitation at various degrees of saturation." *Can. Geotech. J.* 50 (1): 81–90. https://doi.org/10.1139/cgj-2012-0023.

Choi, H. M., and B. Yoo. 2009. "Steady and dynamic shear rheology of sweet potato starch–xanthan gum mixtures." *Food Chem.* 116 (3): 638–643. https://doi.org/10.1016/j.foodchem.2009.02.076.

DeJong, J. T., B. M. Mortensen, B. C. Martinez, and D. C. Nelson. 2010. "Bio-mediated soil improvement." *Ecol. Eng.* 36 (2): 197–210. https://doi.org/10.1016/j.ecoleng.2008.12.029.

Di Lorenzo, F., and S. Seiffert. 2015. "Nanostructural heterogeneity in polymer networks and gels." *Polym. Chem.* 6 (31): 5515–5528. https://doi.org/10.1039/C4PY01677G.

Dzuy, N. Q., and D. V. Boger. 1985. "Direct yield stress measurement with the vane method." *J. Rheol.* 29 (3): 335–347. https://doi.org/10.1122/1.549794.

Eary, L. E., and D. Rai. 1987. "Kinetics of chromium(III) oxidation to chromium(VI) by reaction with manganese dioxide." *Environ. Sci. Technol.* 21 (12): 1187–1193. https://doi.org/10.1021/es00165a005.

Fan, J., K. Wang, M. Liu, and Z. He. 2008. "In vitro evaluations of konjac glucomannan and xanthan gum mixture as the sustained release material of matrix tablet." *Carbohydr. Polym.* 73 (2): 241–247. https://doi.org/10.1016/j.carbpol.2007.11.027.

Fan, Y., J. Yang, A. Duan, and X. Li. 2021. "Pectin/sodium alginate/xanthan gum edible composite films as the fresh-cut package." *Int. J. Biol. Macromol.* 181 (Jun): 1003–1009. https://doi.org/10.1016/j.ijbiomac.2021.04.111.

Farrés, I. F., and I. Norton. 2014. "Formation kinetics and rheology of alginate fluid gels produced by in-situ calcium release." *Food Hydrocolloids* 40 (Oct): 76–84. https://doi.org/10.1016/j.foodhyd.2014.02.005.

Gales, J. R., T. S. Young, G. P. Willhite, and D. W. Green. 1994. "Equilibrium swelling and syneresis properties of xanthan gum/Cr(III) gels." *SPE Adv. Technol. Ser.* 2 (2): 190–198. https://doi.org/10.2118/17328-PA.

García-Ochoa, F., V. Santos, J. Casas, and E. Gomez. 2000. "Xanthan gum: Production, recovery, and properties." *Biotechnol. Adv.* 18 (7): 549–579. https://doi.org/10.1016/S0734-9750(00)00050-1.

Ghoumrassi-Barr, S., and D. Aliouche. 2016. "A rheological study of xanthan polymer for enhanced oil recovery." *J. Macromol. Sci. Part B* 55 (8): 793–809. https://doi.org/10.1080/00222348.2016.1207544.

Gorny, J., G. Billon, C. Noiriel, D. Dumoulin, L. Lesven, and B. Madé. 2016. "Chromium behavior in aquatic environments: A review." *Environ. Rev.* 24 (4): 503–516. https://doi.org/10.1139/er-2016-0012.

Hansen, E. W., and T. Lund. 1995. "Gelation of xanthan in the presence of trivalent chromic ions monitored by proton NMR spin-lattice relaxation. A kinetic study." *J. Phys. Chem.* 99 (24): 9811–9817. https://doi.org/10.1021/j100024a023.

Hansen, J., R. Ruedy, M. Sato, and K. Lo. 2010. "Global surface temperature change." *Rev. Geophys.* 48 (4): RG4004. https://doi.org/10.1029/2010RG000345.

Hatakeyama, H., and T. Hatakeyama. 1998. "Interaction between water and hydrophilic polymers." *Thermochim. Acta* 308 (1–2): 3–22. https://doi.org/10.1016/S0040-6031(97)00325-0.

Im, J., I. Chang, and G.-C. Cho. 2021. "Effects of malonic acid crosslinked starch for soil strength improvement." *Trans. Geotech.* 31 (Nov): 100653. https://doi.org/10.1016/j.trgeo.2021.100653.

Izawa, H., and J.-I Kadokawa. 2010. "Preparation and characterizations of functional ionic liquid-gel and hydrogel materials of xanthan gum." *J. Mater. Chem.* 20 (25): 5235–5241. https://doi.org/10.1039/c0jm00595a.

James, A., D. Williams, and P. Williams. 1987. "Direct measurement of static yield properties of cohesive suspensions." *Rheol. Acta* 26 (5): 437–446. https://doi.org/10.1007/BF01333844.

Jeffrey, G. A., and W. Saenger. 2012. *Hydrogen bonding in biological structures*. Berlin: Springer.

Jeong, S.-W. 2019. "Shear rate-dependent rheological properties of mine tailings: Determination of dynamic and static yield stresses." *Appl. Sci.* 9 (22): 4744. https://doi.org/10.3390/app9224744.

Jia, H., J.-Z. Zhao, F.-Y. Jin, W.-F. Pu, Y.-M. Li, K.-X. Li, and J.-M. Li. 2012. "New insights into the gelation behavior of polyethyleneimine cross-linking partially hydrolyzed polyacrylamide gels." *Ind. Eng. Chem. Res.* 51 (38): 12155–12166. https://doi.org/10.1021/ie301818f.

Jiang, T., J.-D. Zhao, and J. R. Zhang. 2022. "Splitting tensile strength and microstructure of xanthan gum-treated loess." *Sci. Rep.* 12 (1): 1–10. https://doi.org/10.1038/s41598-022-14058-4.

Kang, W., D. Ko, and J. Kang. 2021. "Erosion resistance performance of surface-reinforced levees using novel biopolymers investigated via real-scale overtopping experiments." *Water* 13 (18): 2482. https://doi.org/10.3390/w13182482.

Kang, X., B. Bate, R.-P. Chen, W. Yang, and F. Wang. 2019. "Physico-chemical and mechanical properties of polymer-amended kaolinite and fly ash–kaolinite mixtures." *J. Mater. Civ. Eng.* 31 (6): 04019064. https://doi.org/10.1061/(ASCE)MT.1943-5533.0002705.

Kennedy, J. R., K. E. Kent, and J. R. Brown. 2015. "Rheology of dispersions of xanthan gum, locust bean gum and mixed biopolymer gel with silicon dioxide nanoparticles." *Mater. Sci. Eng., C* 48 (Mar): 347–353. https://doi.org/10.1016/j.msec.2014.12.040.

Ko, D., and J. Kang. 2018. "Experimental studies on the stability assessment of a levee using reinforced soil based on a biopolymer." *Water* 10 (8): 1059. https://doi.org/10.3390/w10081059.

KRCC (Korea Rural Community Corporation). 2001. *Dam grouting design and construction guideline*. Gyeonggi-do, South Korea: KRCC.

Lee, M., J. Im, I. Chang, and G.-C. Cho. 2021a. "Evaluation of Injection capabilities of a biopolymer-based grout material." *Geomech. Eng.* 25 (1): 31–40. https://doi.org/10.12989/gae.2021.25.1.031.

Lee, M., J. Im, G.-C. Cho, H. H. Ryu, and I. Chang. 2021b. "Interfacial shearing behavior along xanthan gum biopolymer-treated sand and solid interfaces and its meaning in geotechnical engineering aspects." *Appl. Sci.* 11 (1): 139. https://doi.org/10.3390/app11010139.

Lee, M., Y.-M. Kwon, D.-Y. Park, I. Chang, and G.-C. Cho. 2022. "Durability and strength degradation of xanthan gum based biopolymer treated soil subjected to severe weathering cycles." *Sci. Rep.* 12 (1): 1–15. https://doi.org/10.1038/s41598-022-23823-4.

Lund, T., O. Smidsrød, B. T. Stokke, and A. Elgsaeter. 1988. "Controlled gelation of xanthan by trivalent chronic ions." *Carbohydr. Polym.* 8 (4): 245–256. https://doi.org/10.1016/0144-8617(88)90064-1.

Marudova-Zsivanovits, M., N. Jilov, and E. Gencheva. 2007. "Rheological investigation of xanthan gum–chromium gelation and its relation to enhanced oil recovery." *J. Appl. Polym. Sci.* 103 (1): 160–166. https://doi.org/10.1002/app.25025.

Moorhouse, R., M. D. Walkinshaw, and S. Arnott. 1977. *Extracellular microbial polysaccharides: A symposium*. Washington, DC: American Chemical Society.

Nolte, H., S. John, O. Smidsrød, and B. T. Stokke. 1992. "Gelation of xanthan with trivalent metal ions." *Carbohydr. Polym.* 18 (4): 243–251. https://doi.org/10.1016/0144-8617(92)90089-9.

Park, S.-S. 2011. "Unconfined compressive strength and ductility of fiber-reinforced cemented sand." *Constr. Build. Mater* 25 (2): 1134–1138. https://doi.org/10.1016/j.conbuildmat.2010.07.017.

Patel, J., B. Maji, N. H. N. Moorthy, and S. Maiti. 2020. "Xanthan gum derivatives: Review of synthesis, properties and diverse applications." *RSC Adv.* 10 (45): 27103–27136. https://doi.org/10.1039/D0RA04366D.

Pelletier, E., C. Viebke, J. Meadows, and P. Williams. 2001. "A rheological study of the order–disorder conformational transition of xanthan gum." *Biopolym. Origin. Res. Biomol.* 59 (5): 339–346. https://doi.org/10.1002/1097-0282(20011015)59:5<339::AID-BIP1031>3.0.CO;2-A.

Pereira, F. C., K. J. Clinckspoor, and R. B. Z. L. Moreno. 2022. "Optimization of an in-situ polymerized and crosslinked hydrogel formulation for lost circulation control." *J. Pet. Sci. Eng.* 208 (Jan): 109687. https://doi.org/10.1016/j.petrol.2021.109687.

Philippova, O. E., A. V. Shibaev, D. A. Muravlev, and D. Y. Mityuk. 2016. "Structure and rheology of solutions and gels of stiff polyelectrolyte at high salt concentration." *Macromolecules* 49 (16): 6031–6040. https://doi.org/10.1021/acs.macromol.6b01392.

Preuss, H. G., and R. A. Anderson. 1998. "Chromium update: Examining recent literature 1997–1998." *Curr. Opin. Clin. Nutr. Metab. Care* 1 (6): 509–512. https://doi.org/10.1097/00075197-199811000-00005.

Prud'homme, R. K., J. T. Uhl, J. P. Poinsatte, and F. Halverson. 1983. "Rheological monitoring of the formation of polyacrylamide/$Cr^{3+}$ gels." *SPE J.* 23 (5): 804–808. https://doi.org/10.2118/10948-PA.

Qureshi, M. U., I. Chang, and K. Al-Sadarani. 2017. "Strength and durability characteristics of biopolymer-treated desert sand." *Geomech. Eng.* 12 (5): 785–801. https://doi.org/10.12989/gae.2017.12.5.785.

Rahbari, R., and J. Francois. 1992. "Interactions between aluminium ions and acrylic acid-acrylamide copolymers in aqueous solution: 3. Influence of ionic strength on gelation and phase separation." *Polymers* 33 (7): 1449–1458. https://doi.org/10.1016/0032-3861(92)90121-C.

Riaz, T., M. W. Iqbal, B. Jiang, and J. Chen. 2021. "A review of the enzymatic, physical, and chemical modification techniques of xanthan gum." *Int. J. Biol. Macromol.* 186 (Sep): 472–489. https://doi.org/10.1016/j.ijbiomac.2021.06.196.

Rodd, A. B., D. E. Dunstan, D. V. Boger, J. Schmidt, and W. Burchard. 2001. "Heterodyne and nonergodic approach to dynamic light scattering of polymer gels: Aqueous xanthan in the presence of metal ions (aluminum (III))." *Macromolecules* 34 (10): 3339–3352. https://doi.org/10.1021/ma001706g.

Sanderson, G. R. 1981. "Applications of xanthan gum." *Br. Polym. J.* 13 (2): 71–75. https://doi.org/10.1002/pi.4980130207.

Seo, S., M. Lee, J. Im, Y.-M. Kwon, M.-K. Chung, G.-C. Cho, and I. Chang. 2021. "Site application of biopolymer-based soil treatment (BPST) for slope surface protection: In-situ wet-spraying method and strengthening effect verification." *Constr. Build. Mater.* 307 (Nov): 124983. https://doi.org/10.1016/j.conbuildmat.2021.124983.

Sethi, S., B. S. Kaith, M. Kaur, N. Sharma, and V. Kumar. 2020. "Cross-linked xanthan gum–starch hydrogels as promising materials for controlled drug delivery." *Cellulose* 27 (8): 4565–4589. https://doi.org/10.1007/s10570-020-03082-0.

Shibaev, A. V., D. A. Muravlev, A. K. Muravleva, V. V. Matveev, A. E. Chalykh, and O. E. Philippova. 2020. "pH-dependent gelation of a stiff anionic polysaccharide in the presence of metal ions." *Polymers* 12 (4): 868. https://doi.org/10.3390/polym12040868.

Singh, S. P., and R. Das. 2020. "Geo-engineering properties of expansive soil treated with xanthan gum biopolymer." *Geomech. Geoeng.* 15 (2): 107–122. https://doi.org/10.1080/17486025.2019.1632495.

Soldo, A., M. Miletić, and M. L. Auad. 2020. "Biopolymers as a sustainable solution for the enhancement of soil mechanical properties." *Sci. Rep.* 10 (1): 267. https://doi.org/10.1038/s41598-019-57135-x.

Song, K.-W., Y.-S. Kim, and G.-S. Chang. 2006. "Rheology of concentrated xanthan gum solutions: Steady shear flow behavior." *Fibers Polym.* 7 (2): 129–138. https://doi.org/10.1007/BF02908257.

Stokes, J., and J. Telford. 2004. "Measuring the yield behaviour of structured fluids." *J. Non-Newtonian Fluid Mech.* 124 (1–3): 137–146. https://doi.org/10.1016/j.jnnfm.2004.09.001.

Sujatha, E. R., S. Atchaya, A. Sivasaran, and R. S. Keerdthe. 2020. "Enhancing the geotechnical properties of soil using xanthan gum—An eco-friendly alternative to traditional stabilizers." *Bull. Eng. Geol. Environ.* 80 (Feb): 1157–1167. https://doi.org/10.1007/s10064-020-02010-7.

Tran, A. T. P., I. Chang, and G.-C. Cho. 2019. "Soil water retention and vegetation survivabiity improvement using microbial biopolymers in drylands." *Geomech. Eng.* 17 (5): 475–483. https://doi.org/10.12989/gae.2019.17.5.475.

Wang, Z. Y., Q. Z. Zhang, M. Konno, and S. Saito. 1994. "Sol–gel transition of alginate solution by the addition of various divalent cations: A rheological study." *Biopolymers* 34 (6): 737–746. https://doi.org/10.1002/bip.360340606.

Whiffin, V. S., L. A. van Paassen, and M. P. Harkes. 2007. "Microbial carbonate precipitation as a soil improvement technique." *Geomicrobiol. J.* 24 (5): 417–423. https://doi.org/10.1080/01490450701436505.

Worrell, E., L. Price, N. Martin, C. Hendriks, and L. O. Meida. 2001. "Carbon dioxide emissions from the global cement industry." *Annu. Rev. Energy Environ.* 26 (1): 303–329. https://doi.org/10.1146/annurev.energy.26.1.303.

Zhang, G., L. Chen, J. Ge, P. Jiang, and X. Zhu. 2015. "Experimental research of syneresis mechanism of HPAM/Cr3+ gel." *Colloids Surf. Physicochem. Eng. Aspects* 483 (Oct): 96–103. https://doi.org/10.1016/j.colsurfa.2015.07.048.

Zhang, Z., H. Pan, P. Liu, M. Zhao, X. Li, and Z. Zhang. 2017. "Boric acid incorporated on the surface of reactive nanosilica providing a nanocrosslinker with potential in guar gum fracturing fluid." *J. Appl. Polym. Sci.* 134 (27): 45037. https://doi.org/10.1002/app.45037.

Zheng, C., Q. Yang, and J. Huang. 2019. "Lignin with and without polymerization for soil stabilization." *J. Mater. Civ. Eng.* 31 (12): 04019292. https://doi.org/10.1061/(ASCE)MT.1943-5533.0002935.

Zolfaghari, R., A. A. Katbab, J. Nabavizadeh, R. Y. Tabasi, and M. H. Nejad. 2006. "Preparation and characterization of nanocomposite hydrogels based on polyacrylamide for enhanced oil recovery applications." *J. Appl. Polym. Sci.* 100 (3): 2096–2103. https://doi.org/10.1002/app.23193.